

Flexible and Scalable Deep Dendritic Spiking Neural Networks with Multiple Nonlinear Branching

Yifan Huang^{1,3}, Wei Fang², Zhengyu Ma³, Guoqi Li^{4*}, Yonghong Tian^{1,2,3*}

¹School of Computer Science, Peking University, Beijing, China.

²School of Electronic and Computer Engineering, Shenzhen Graduate School, Peking University, Shenzhen, China.

³Peng Cheng Laboratory, Shenzhen, China.

⁴Institute of Automation, Chinese Academy of Sciences, Beijing, China.

*Corresponding author(s). E-mail(s): guoqi.li@ia.ac.cn; yhtian@pku.edu.cn;

Abstract

Recent advances in spiking neural networks (SNNs) have a predominant focus on network architectures, while very little attention has been paid to the underlying neuron model. The point neuron models, a cornerstone of existing deep SNNs, pose a bottleneck on the network-level expressivity since they depict somatic dynamics only. In contrast, the multi-compartment models in neuroscience offer remarkable expressivity and biological plausibility by introducing dendritic morphology and dynamics, but remain underexplored in deep learning due to their unaffordable computational overhead and inflexibility. To combine the advantages of both sides for a flexible, efficient yet more powerful computational model, we propose the dendritic spiking neuron (DendSN) incorporating multiple dendritic branches with nonlinear dynamics. Compared to the point spiking neurons, DendSN exhibits significantly higher expressivity. DendSN’s flexibility enables its seamless integration into diverse deep SNN architectures. To accelerate dendritic SNNs (DendSNNs), we parallelize dendritic state updates across time steps, and develop Triton kernels for GPU-level acceleration. As a result, we can construct various large-scale DendSNNs with depth comparable to their point SNN counterparts. Next, we comprehensively evaluate DendSNNs’ performance on various demanding tasks. We first propose a novel algorithm called dendritic branch gating (DBG) for continual learning. By modulating dendritic branch strengths using an additional task context signal, DBG significantly mitigates catastrophic forgetting of DendSNNs. Moreover, DendSNNs demonstrate enhanced robustness against noise and adversarial attacks compared to point SNNs, and excel in few-shot learning settings. Our work firstly demonstrates the possibility of training bio-plausible dendritic SNNs with depths and scales comparable to traditional point SNNs, and reveals superior expressivity and robustness of reduced dendritic neuron models in deep learning, thereby offering a fresh perspective on advancing neural network design.

Keywords: Dendritic Computing, Deep Spiking Neural Networks, Dendritic Modulation, Multi-compartment Models, Network-level Expressivity

Introduction

The past decade has witnessed the success of deep learning across diverse domains, including computer vision [1, 2], natural language processing [3–5], and autonomous driving [6, 7]. With the surge in the performance of parallel computing devices like GPUs, increasingly deeper artificial neural networks (ANNs) with meticulously crafted architectures can be efficiently trained and conveniently deployed for real-world applications [8–10]. In addition, inspired by the information processing mechanisms of biological neural circuits, spiking neural networks (SNNs) have emerged as a potentially more bio-plausible and energy-efficient alternative to ANNs [11, 12]. Recent advances in neuromorphic hardware [13–15] and SNN programming frameworks [16–18] have

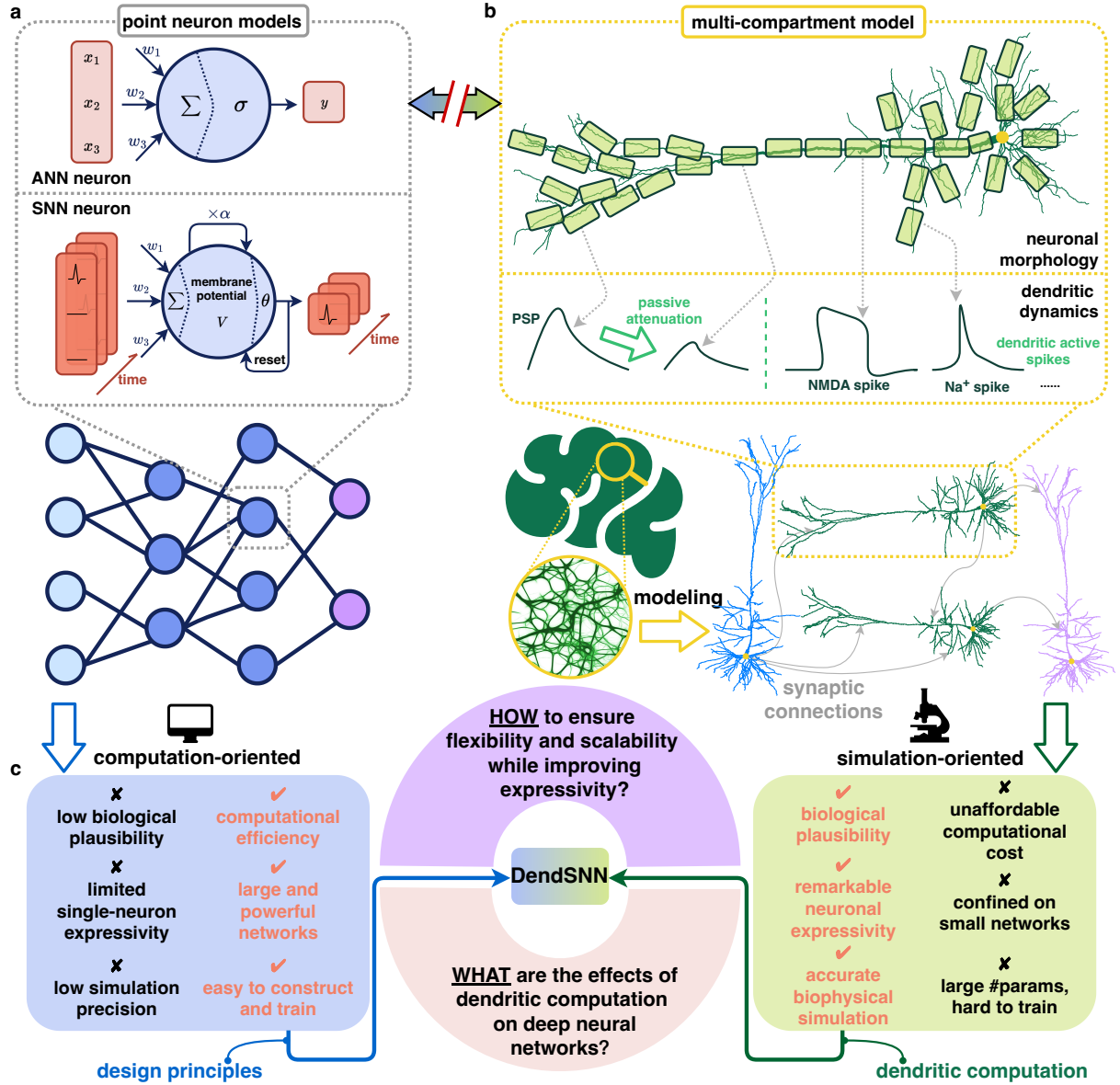


Figure 1 A comparison between deep neural networks with point neurons and biophysical neural network models with multi-compartment neurons. **a)** Typically, deep neural networks (lower) adopt point neuron models (upper) as their basic computational units. Both the perceptron in deep ANNs and the LIF model in deep SNNs belong to this category. They simplify the neuron’s morphology to a single spatial point. **b)** Multi-compartment models (upper) in neuroscience capture the detailed morphologies of real neurons and have complex dendritic dynamics. By connecting these intricate neurons, biophysical network models (lower) are established to simulate small-scale neural circuits in the brain. Notice that there may be multiple synaptic connections between a pair of neurons. **c)** Deep neural networks based on point neurons are computationally efficient and convenient to construct and train, but fall short on bio-plausibility and single-neuron expressivity (blue box). Biophysical networks with multi-compartment neurons have remarkable expressivity and can simulate the complex properties of real neurons, but cannot be easily scaled up to large networks (green box). There is a gap between these two types of models. In this work, we propose DendSNN and DendSNN, combining dendritic computation with the design principles of deep learning to power up deep SNNs. We mainly focus on two questions: *how* to ensure model flexibility and scalability while improving expressivity, and *what* the effects of dendritic computation on deep neural networks are in diverse machine learning scenarios.

further fueled the interest in deep SNNs, positioning them as promising models for the next generation of neural networks [19].

The fundamental issue in modern SNN researches is to combine spiking neuronal dynamics with deep network architectures and further identify the most suitable application scenarios. Cutting-edge studies in this field are leveraging ANN building blocks like residual connections [2] and self-attention mechanisms [3]

for building up their spiking variants [20–26], powering up deep SNNs and yielding enhanced performance. However, much less attention is directed towards the intricacies of the underlying neuron model. Previous studies in neuroscience have found that the computational expressivity of a single biological neuron rivals that of a multi-layer neural network consisting of thousands of artificial neurons [27–30]. This suggests an urgent need to rethink the design of individual neurons in deep neural networks, and biological neurons may serve as a valuable source of inspiration for possible enhancements. Nevertheless, how to integrate the remarkable expressivity of biological neurons into neurons of deep neural networks for improved performance in practical tasks remains to be explored.

The dynamic mechanisms of biological neurons arise mainly from two sources: dendritic computations and somatic dynamics. Most existing deep SNNs, however, are built upon oversimplified neurons such as the leaky integrate-and-fire (LIF) model [31], treating the entire neuron as a single spatial point and only depicting the dynamic properties of the soma. Models like the parametric leaky integrate-and-fire (PLIF) neuron [32] and the few-spikes neuron (FS-neuron) [33] attempt to enhance neuron-level dynamics by introducing learnable internal parameters, but still fail to take dendrites into account. These spiking neuron models, as well as their non-spiking counterparts in ANNs [34], are termed **point neuron models** due to their reduced morphology and dynamics (Figure 1a). Notwithstanding their computational efficiency and reduced memory usage, these prevalent models sacrifice essential computational properties of dendrites, resulting in limited single-neuron expressivity. The oversimplification of point neuron models is a bottleneck that constrains the overall expressivity of deep SNNs and hinders the networks’ ability to perform intricate computations for challenging tasks, as summarized within the blue box in Figure 1c.

In stark contrast, neuroscientists use interconnected **multi-compartment models** to simulate the biophysical activities of small-scale neuron circuits in the brain [35, 36]. As illustrated in Figure 1b, multi-compartment models portray neuronal morphology at a fine granularity, and use differential equations with hundreds of variables to describe neuronal dynamics [37–39]. They manage to capture critical computational properties present in biological dendrites [40–42], including the passive attenuation of input signals [43], the active generation of dendritic spikes [44], as well as the selection and multiplexing of information [41]. As a result, multi-compartment models exhibit remarkable neuron-level expressivity (Figure 1c, green box). Adding structural complexity and dendritic nonlinear dynamics to the neurons in deep SNNs is thus an intuitive and promising strategy for elevating the networks’ expressivity and performance. The research community, however, has overlooked the role of dendritic computation in deep SNNs so far.

The idea of incorporating dendritic computation into deep learning, nonetheless, poses challenges related to network scalability and model flexibility. The success of deep learning models is primarily attributed to their large scales and intricate architectures. However, simulating large populations of multi-compartment neurons with complex dynamics is computationally prohibitive; even if these models can be simplified to reduce computational overhead, they are not trivially compatible with today’s complex network architectures (see Figure 1c, green box). For instance, some pioneering works focusing on bio-plausibility encounter scalability difficulties as network sizes increase due to the burden of solving differential equations for complicated neuronal dynamics [45–47]. A recent study by Zheng et al. [48] simplifies multi-compartment models and proposes the DH-LIF neuron with temporal dendritic heterogeneity. They manage to build fully connected dendritic SNNs with recurrent connections and achieve competitive performances on tasks with rich timescales. Nevertheless, their neuron model has not been applied to networks with more than five layers due to high computational overhead, nor has it extended to prevalent SNN architectures like convolutional networks and Transformers. Some ANN neurons incorporate properties of dendritic computation [49–51] while neglecting temporal dynamics. Yet, they remain confined to small-scale fully connected networks. Thus, the fundamental question of *how* to ensure model flexibility and scalability while improving neuron-level expressivity is still unresolved (Figure 1c, upper part of the ring). We emphasize the necessity of adapting dendritic neurons to diverse network architectures; we also claim that two core requirements must be met to overcome the scalability issues: (1) developing a dendritic neuron model with highly parallelized simulation algorithms, and (2) leveraging the computational power of modern GPUs through low-level programming languages. Tackling these challenges is crucial and imperative for the practical applications of dendritic neural networks to complicated tasks.

Furthermore, while dendritic computation has been extensively studied [39–41, 52, 53], its influences on deep neural networks remain largely unexplored. Most previous works narrowly focus on one aspect of dendrites’ benefits to deep learning, lacking a comprehensive study on the diverse network-level impact of dendrites in various machine learning scenarios [45, 47–49, 51]. As demonstrated in the middle of Figure 1c, understanding the influence of dendritic computation on deep neural networks in diverse task settings is another critical issue that needs to be resolved.

To address these challenges, we propose the dendritic spiking neuron (DendSN) model that incorporates multiple dendritic branches with nonlinear dynamics. We demonstrate that DendSN has significantly higher expressivity than point spiking neurons, mainly due to its enhanced dendritic branch weighting mechanism. An acceleration algorithm is further proposed to parallelize dendritic dynamics computation over time, making the extra overhead negligible compared to point spiking neurons. We then introduce a universal solution to seamlessly integrate DendSNs into various deep SNN architectures, showcasing the flexibility of our model. Triton kernels [54] are developed to fully exploit the power of GPUs, enabling dendritic spiking neural networks (DendSNNs) to reach the same depths as traditional deep SNN architectures while keeping affordable computational costs. DendSNNs are compatible with existing large-scale SNN training methods, and demonstrate improved accuracies compared to point SNNs in static image and event-based data classification tasks, even without introducing extra learnable parameters. We next comprehensively evaluate DendSNNs’ performances across various settings to show their superior network-level expressivity and robustness compared to point SNNs. Inspired by dendritic modulation mechanism and synaptic clustering phenomenon observed in biological neural circuits [55–57], we propose dendritic branch gating (DBG), a novel algorithm designed for continual learning. By adjusting dendritic branch strengths based on task context signals, DBG effectively reduces interference between synaptic inputs from different tasks. Moreover, additional experiments reveal that DendSN can enhance the robustness of SNNs against noise and adversarial attacks, with improved performances also observed in few-shot learning scenarios. To the best of our knowledge, this is the first work that demonstrates the possibility and feasibility of constructing and training SNNs incorporating multiple nonlinear dendritic branches with depth and scale comparable to traditional deep SNNs, and conducts a systematic study on the benefits of dendritic computation for deep networks in diverse machine learning scenarios.

Results

Balancing expressivity and computational cost of dendritic spiking neuron

Distinguishing themselves from point neuron models widely employed in deep learning, multi-compartment models in computational neuroscience incorporate internal spatial structures and neuronal dynamics, as demonstrated in Figure 1b. These intricate models depict neuronal morphology at a micrometer level and portray nonlinear dynamics using an extensive set of variables [37–39], hence being capable of capturing complex behavior patterns of biological neurons. Nevertheless, their computational complexity impedes their application in deep neural networks, even with optimal acceleration methods in place [58]. In response, reasonable simplifications are imperative to simulate a large population of complex neurons while preserving essential structural and computational properties.

We propose the dendritic spiking neuron (DendSN) model illustrated in Figure 2b to strike this delicate balance. The simulation process is carried out over T discrete time steps using the Euler method, just as the standard practice in SNNs. Structurally, the neuron comprises B parallel dendritic branches and a soma. The i -th dendritic branch possesses a single state variable V_i^d , representing the dendritic local potential. At each time step t , the potential undergoes an update based on synaptic input X_i , and decays exponentially over time with a factor α .

$$V_i^d[t] = \alpha V_i^d[t-1] + X_i[t] \quad (1)$$

$V_i^d[t]$ is then activated by a nonlinear function f_i and subsequently weighted by a factor $K_{t,i}$, yielding the branch-to-soma signal $Y_i[t]$. The total input to the soma is the sum of the signals from all the branches.

$$Y[t] = \sum_{i=0}^{B-1} Y_i[t] = \sum_{i=0}^{B-1} K_{t,i} f_i(V_i^d[t]), \quad t \in \{0, \dots, T-1\} \quad (2)$$

Finally, the soma is a LIF neuron with a unary state variable V^s as the somatic membrane potential [31]. It charges through the aggregated dendrite-to-soma signal Y , decays exponentially with a factor β , emits a spike when V^s exceeds a threshold V_{th}^s , and resets to V_{reset}^s after firing. The somatic dynamics can be described as

$$\begin{aligned} H^s[t] &= \beta V^s[t-1] + (1 - \beta)Y[t] \\ S[t] &= \Theta(H^s[t] - V_{th}^s) \\ V^s[t] &= (1 - S[t])H^s[t] + S[t]V_{reset}^s \end{aligned} \quad (3)$$

where H^s is the somatic potential before spike emission, and Θ is the Heaviside step function.

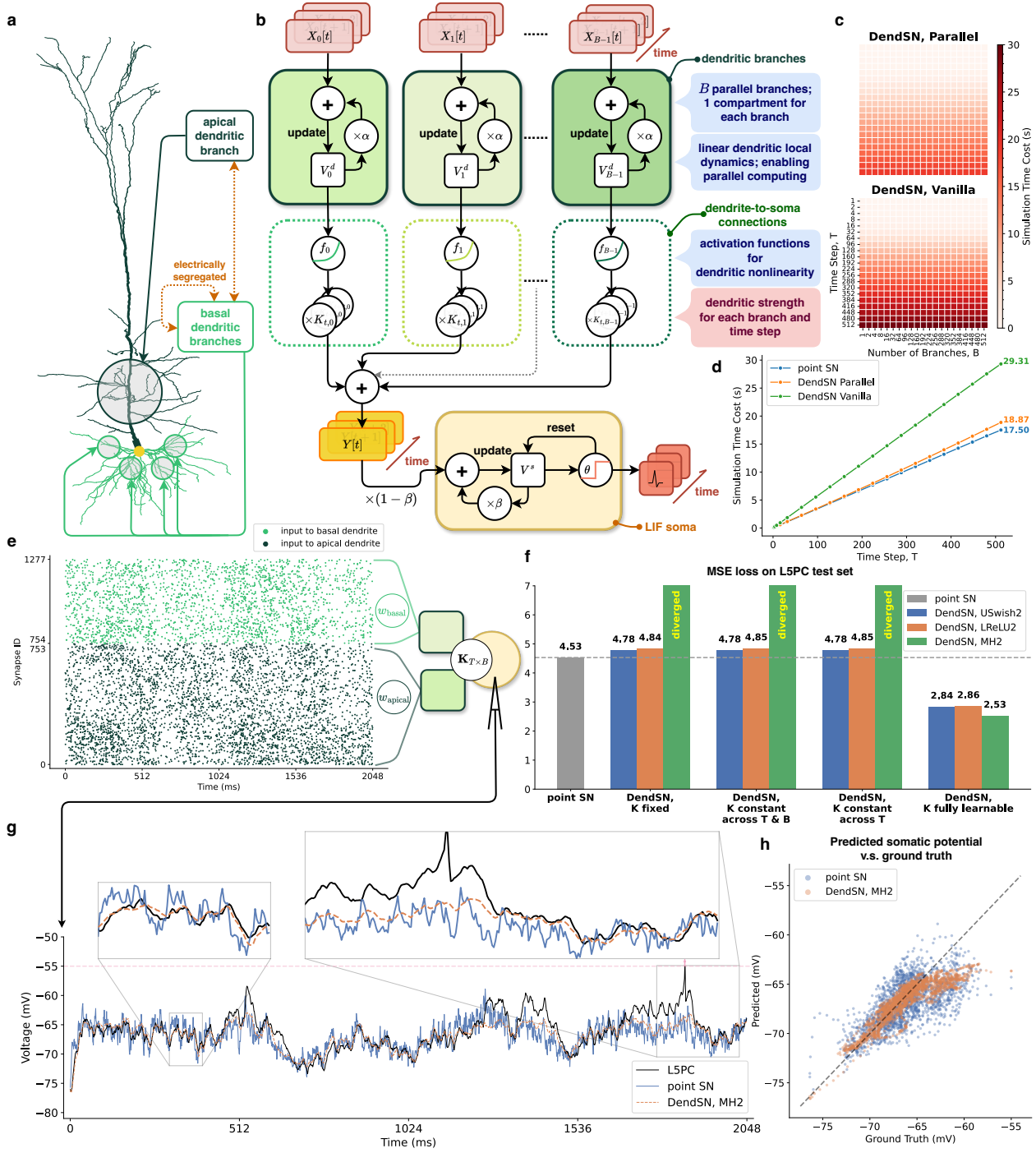


Figure 2 The DendSN model and its simulation results. **a)** A schematic illustration of a rat layer-5 pyramidal cell’s (L5PC) morphology [30]. **b)** Our proposed DendSN model. It simplifies a multi-compartment model from three aspects: spatial structure, local dynamics, and signal transmission mechanism (blue boxes). A strength value is assigned to each dendritic branch at each time step, greatly enhancing the model’s expressivity (red box). **c), d)** The computational overhead of different neuron models on a GPU. Here, “DendSN, Parallel” means a DendSN whose dendritic dynamics are computed in parallel across both time and branches, while “DendSN, Vanilla” is a DendSN simulated with the vanilla Euler method. “Simulation time cost” refers to the total time required to sequentially process 512 randomly generated input samples of length T . The data in Subfigure d is obtained by averaging the time costs along all the conditions of B while keeping the T conditions. **e)** An illustration of the L5PC fitting experiment. For DendSN conditions, B is set to 2, representing the apical and basal dendrites. The presynaptic spikes are weighted by synaptic strengths, summed, and then fed into the branches. Parameters in the circles are optimized using gradient descent. For point SN conditions, the weighted sum of all the spikes is directly fed into the soma. **f)** The fitting losses of different models on the test set. Here, “USwish2” means USwish dendritic nonlinear activation (see Methods) and $B = 2$. **g), h)** The somatic membrane potential of a detailed multi-compartment L5PC model (black, ground truth), a point neuron model (blue), and a DendSN with a fully learnable branch strength matrix (orange, dashed). The trial is selected from the test set.

Compared to detailed multi-compartment neurons, DendSN makes simplifications on spatial structure, source of nonlinearity, and dendritic local dynamics to reduce its computational complexity (see the blue boxes in Figure 2b). Firstly, the dendritic tree is portrayed as B electrically segregated branches, each modeled as a single compartment. This abstraction is a nod to the common presence of multiple dendritic branches in biological neurons like pyramidal cells [59, 60] (Figure 2a) while intentionally forgoing intricate morphological details. It not only significantly reduces memory costs for representing neuronal morphology, but also eliminates the need for transmitting signals between dendritic compartments, improving simulation efficiency. Secondly, nonlinear branch activation functions $\mathcal{F} = \{f_i\}_{i=0}^{B-1}$ are introduced to directly map dendritic states to branches’ overall contributions to somatic potential change (see Supplementary Information S1 for more details). Dendritic nonlinearity, one of the key computational properties of dendritic computation, is attached to the model in a general manner by these element-wise functions. Hence, we don’t have to explicitly model the complex biophysical processes of gated dendritic ion channels using additional state variables and simulate their dynamics at high temporal resolution. Thirdly, since all the nonlinear components are shifted to the dendrite-to-soma signal forwarding process, the local dynamics of each dendritic state V_i^d remain completely linear, merely reflecting passive electrical property [41, 43]. Thanks to their linearity, dendritic states can be updated in parallel across different branches as well as time steps. The acceleration algorithm of dendritic state computation is further explained by Equation (14) and (15) in Methods.

Under these simplifications, DendSN can be simulated with high efficiency on parallel computing devices like GPUs. As shown in Figure 2c, the simulation time cost of DendSN remains almost constant as the number of dendritic branches B increases, whether the acceleration of dendritic state update is applied or not. We attribute the constancy to the parallel arrangement of dendritic compartments, which allows for simultaneous updates of all the B dendritic states. Detailed multi-compartment models with B dendritic compartments, by contrast, inevitably suffer from a noticeable increase in simulation time cost as B grows, since the state of a particular compartment depends on the states of all its parent nodes [58]. Apart from that, Figure 2d suggests that the simulation time costs of both point neuron and DendSN grow linearly with the number of time steps T . If the parallelism of dendritic state update across time is exploited, DendSN’s simulation efficiency can be boosted to a level almost identical to that of the point neuron. Thus, the extra computational load imposed by dendrites is negligible in practice. These observations indicate that DendSN is computationally more affordable than conventional multi-compartment models, and holds promise for application in deep neural networks.

Despite its relatively low computational cost, DendSN retains a remarkable expressivity, mainly due to the enhancement of the branch weighting mechanism (see the red box in Figure 2b). The branch strength matrix $\mathbf{K} = [K_{t,i}]_{T \times B}$ assigns weights to different branches at different time steps, having the capacity to model the complex dependency of the somatic potential on dendritic states. To show that $\mathbf{K}_{T \times B}$ is the key factor endowing DendSN with the ability to capture crucial computational properties of biological neurons, we conduct a fitting experiment using activity data from a multi-compartment biophysical model of a layer-5 pyramidal cell [30], as illustrated in Figure 2e. By leveraging gradient descent to learn both the synaptic weights and \mathbf{K} (if DendSN is used), a single reduced neuron model can approximate the mapping from presynaptic spikes to somatic membrane potential of the detailed model. Figure 2f demonstrates that DendSNs with fully learnable \mathbf{K} can achieve significantly better performances than a point LIF model, regardless of the dendritic activation function used. DendSN with non-monotonic Mexican hat dendritic nonlinearity yields the lowest mean squared error (MSE) on the test set, about 56% of LIF neuron’s MSE. However, if \mathbf{K} ’s degree of freedom is restricted by setting it as a constant matrix or enforcing its rows or columns to be identical, the approximation and generalization performance of DendSN will degrade to LIF’s level. To be worse, models with Mexican hat dendritic activation function may fail to converge on the training set under these constraints. In Figure 2g, we visualize the potential sequences of the original biophysical model (black), a LIF neuron (blue), and a DendSN with fully learnable \mathbf{K} and Mexican hat activation (orange, dashed), given the same input spike train. Notably, DendSN approximates the ground truth with high fidelity when the somatic potential is far below the firing threshold, while the potential of the point neuron fluctuates severely and deviates from the ground truth. The smoothness of DendSN’s potential trace is a direct result of its passive dendritic dynamics, which proves to be beneficial in this task. Although DendSN fails to predict the potential when the ground truth is close to the firing threshold (see the upper right box in Figure 2g, as well as Figure 2h), the decent performance in the subthreshold regime indicates DendSN’s solid biological plausibility and marvelous expressivity.

In summary, DendSN stands as a streamlined yet expressive model for dendritic neurons. The branch weighting mechanism enhances the neuron’s capacity, while the simplifications of dendritic morphology and nonlinear dynamics enable parallel computation across branches and time, reducing computational overhead. Its excellent expressivity and efficiency make it suitable for deep learning applications.

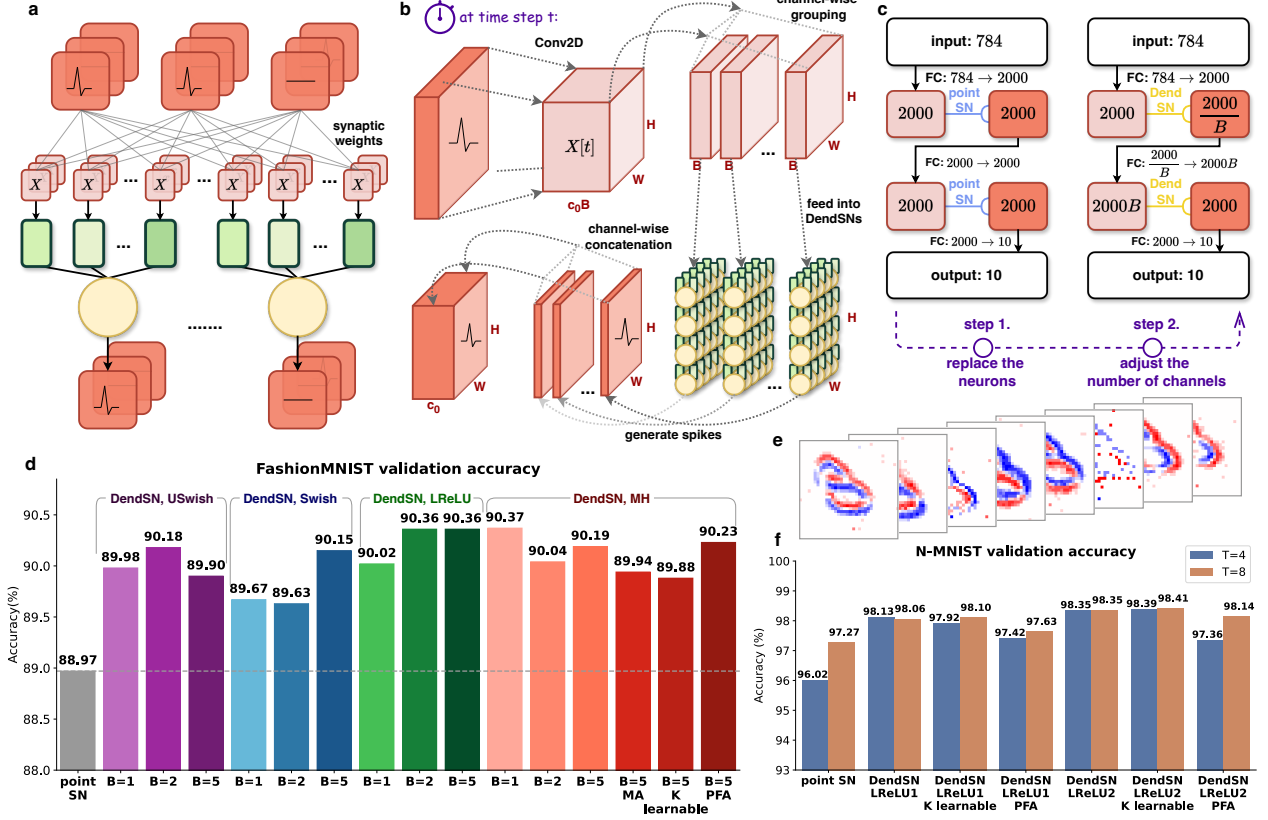


Figure 3 Dendritic spiking neural networks and their supervised learning performance. a),b) Detailed illustrations showcasing how input features \mathbf{X} are assigned to different dendritic branches of a DendSN layer following either a fully connected layer (Subfigure a) of a 2D convolutional layer (Subfigure b). c) A comparison between a fully connected point SNN and a DendSNN with similar architecture. By replacing the point neuron layers with DendSN layers and adjusting the number of channels, a point SNN architecture can be easily converted to a DendSNN. d) Classification accuracies on the FashionMNIST benchmark. DendSNNs consistently outperform point SNNs, no matter which dendritic activation functions are used, how many dendritic branches are employed, and how branch strength matrices are set. e) A sample from the event-based N-MNIST dataset. f) Classification accuracies on the N-MNIST dataset. DendSNNs achieve better performances than point SNNs on different time resolution settings ($T = 4, 8$).

Dendritic spiking neural networks and their supervised training

The efficacy of modern deep learning stems from the vast scale and well-crafted structure of neural networks. Deep network architectures like ResNet [2] and Transformer [3] have been widely embraced for tackling machine learning problems in diverse domains. Pioneering works in the field of SNN have leveraged these advantageous design principles and built up their spiking counterparts, outperforming those plain and shallow SNNs [20–26]. Here, we integrate our DendSN into various deep SNNs with commonly used architectures, aiming to fully harness both the expressive power of DendSN and the capabilities of deep networks for tackling complex tasks.

To embed DendSNs into deep SNNs, an ensemble of neurons is first organized as a layer to facilitate tensor-based parallel simulation. For simplicity, we assume that all DendSNs in the layer share the same neuronal parameters $\alpha, \mathcal{F}, \beta$, except for the branch strength matrix \mathbf{K} . By default, all the neuronal parameters stay constant during both training and inference to avoid introducing extra learnable weights. The DendSN layer is positioned after a weight layer, forming a weight-DendSN block. The weight layer acts as synaptic connections; unlike previous works on dendritic deep learning, we do not impose an explicit sparsity constraint on the weight layer [48, 49] for the sake of simplicity and computational efficiency (see S3 for more details). The output of the weight layer is then folded along the channel (feature map) dimension into B folds, where the i -th fold serves as the input to the i -th branch of all DendSNs in this layer.

$$\mathbf{X}_i^{(c)} = \tilde{\mathbf{X}}^{(cB+i)}, i \in \{0, \dots, B-1\} \quad (4)$$

Here, $\tilde{\mathbf{X}}^{(cB+i)}$ denotes the $(cB+i)$ -th feature map of the weight layer’s output, and $\mathbf{X}_i^{(c)}$ represents the input to the i -th dendritic branch of all DendSNs at channel c in this layer (refer to Methods for detailed explanations).

Consequently, a DendSN layer reduces the number of feature maps to $1/B$ of its original value, while retaining the size of the spatial dimensions. Note, Equation (4) provides a universal solution to the input feature assignment problem for DendSN layers after different types of weight layers. Figure 3a and Figure 3b demonstrate two specific cases for fully connected and 2D convolutional layers, respectively. Supplementary Information S2 provides PyTorch implementations of a DendSN layer, either accelerated using temporal parallelism mentioned in the last section or not.

By cascading multiple weight-DendSN blocks, a deep DendSNN can be established. In fact, nearly all prevalent SNN designs can be converted to their DendSNN counterparts, thanks to the flexibility of the DendSN layer design as described in Equation (4). From the perspective of deep learning, DendSN layers serve as nonlinear activation functions, akin to the role point spiking neuron layers play in traditional SNNs. The main difference lies in the $1/B$ feature compression introduced by a layer of B -branch DendSNs. Therefore, a DendSNN architecture can be intuitively built up by first replacing the point spiking neuron layers in a conventional SNN with DendSN layers, and then adjusting the number of feature maps in the weight layers to align with the requirements of DendSN layers, as Figure 3c suggests. This process can be implemented by popular deep learning frameworks like PyTorch [61] in a plug-and-play manner, making DendSNNs highly accessible and flexible for deep learning practitioners.

In addition to flexibility, computational efficiency is a crucial requirement for deep DendSNNs. As illustrated in Figure 2d from the previous section, DendSN achieves low simulation cost by enabling parallel dendritic state updates both across branches and over time. This parallelism forms the algorithmic foundation for the efficient computation of deep DendSNNs. We also employ hand-crafted Triton kernels [54] to leverage the full power of GPUs. This combination of algorithmic improvement and GPU-level acceleration allows DendSNNs to be trained and evaluated with high efficiency, ensuring their scalability for large-scale tasks.

The dynamics of a DendSN layer are fully differentiable, except for the Heaviside step function in the spike generation process. This issue can be circumvented using surrogate gradient [62, 63], a common practice in directly trained point SNNs. Hence, DendSNNs can be trained in a supervised manner using gradient-based optimization methods like spatio-temporal backpropagation (STBP, a special case of BPTT) [64], enabling them to tackle a wide range of complex tasks. Here, we use two toy datasets to show the feasibility of training DendSNNs; in later sections, we will train DendSNNs with depths and scales comparable to prevalent deep point SNNs to solve more challenging tasks. By optimizing synaptic weights, 3-layer fully connected DendSNNs can achieve persistently better classification accuracies on the FashionMNIST [65] dataset, compared to a point SNN with a similar architecture and equal number of learnable parameters, no matter which dendritic activation function and how many dendritic branches are employed (Figure 3d). Moreover, the expressivity of DendSNNs can be further augmented by appropriately setting the branch strength matrices \mathbf{K} for each DendSN in the network. We introduce three advanced models for setting up the strength matrices: direct learning, CBAM-based multi-dimensional attention on dendrite-to-soma signal (MA) [66], and SimAM-inspired parameter-free attention (PFA) [67]. Experiments on FashionMNIST indicate that PFA marginally improves the classification accuracy of DendSNN with 5 branches and Mexican hat dendritic activation (see Figure 3d) even though no extra learnable parameters are brought in. The other two methods, in contrast, slightly degrade the model’s generalization performance. Further experiments are conducted on the event-based N-MNIST [68] dataset (Figure 3e) using a convolutional network structure, under different temporal resolutions. Figure 3f reveals a trend similar to that of FashionMNIST, except for the fact that learning \mathbf{K} directly improves models’ performance whereas PFA does not. For more information about the results of the experiments, refer to Table S2 and S3. Notice that DendSNNs with MA cannot converge on the N-MNIST training set, so it is omitted from the figure. Our experience suggests that MA works on small fully connected DendSNNs with large B , while larger convolutional DendSNNs with MA mechanism and a small B value are hard to train with MA at the beginning.

All in all, the flexibility and efficiency of DendSN make the construction of large-scale DendSNNs possible. DendSNNs can achieve better performance on supervised learning tasks than point SNNs, even without introducing extra learnable parameters. The superiority of DendSNNs on ordinary supervised learning tasks is the basis for their application in more challenging scenarios.

Dendritic modulation for continual learning

Having presented our solution to incorporate dendritic computation into deep networks and the fact that DendSNNs exhibit remarkable expressivity, we now attempt to explore dendritic computation’s influence on deep neural networks in demanding machine learning settings. Our initial focus is on continual learning, where a model should sequentially adapt to multiple data distributions without forgetting previously learned tasks. This ability is inherent in biological intelligence, reflecting the resilience of nervous systems. However, it poses

a major challenge for artificial intelligent systems [69]. We argue that catastrophic forgetting of previously acquired knowledge can be alleviated by leveraging dendritic computation in a bio-inspired manner.

In the brain, sensory neurons receive not only bottom-up feedforward inputs but also top-down modulatory signals that adjust neuronal activity patterns [70]. These modulation inputs, typically originating from motor and prefrontal areas, encode higher-level information such as task context [71, 72], thus bringing task-specific properties to sensory processing. Wybo et al. [55] revealed that NMDA-driven dendritic spikes may underlie contextual modulation of hierarchical sensory pathways, directing our attention to the role of dendritic modulation in task incremental learning.

What’s more, the spatial location of synaptic sites on the dendritic tree greatly influences a biological neuron’s response to synaptic inputs [73, 74]. A pertinent hypothesis is **synaptic clustering**, which suggests that functionally related synapses tend to cluster on dendrites as the result of structural plasticity, as shown in Figure 4a. Previous studies have revealed that synaptic clusters are vital for increasing the brain’s memory storage capacity [75], as functionally related inputs are preprocessed locally at the dendritic tree before integration at the soma, reducing interference from less relevant inputs. This hypothesis is supported by a wide range of anatomical and computational evidence [56, 57, 76].

Inspired by dendritic modulation and synaptic clustering, we propose a novel algorithm named **dendritic branch gating (DBG)** to mitigate catastrophic forgetting of DendSNNs in task-incremental learning scenarios (see Figure 4b and Supplementary Information S5). The index of the current task, denoted as q , serves as a top-down modulation signal and is fed to the network alongside the feedforward input during both training and inference. Note that the use of an extra context signal is a common practice in previously proposed architecture-based continual learning algorithms like XdG [77]. However, instead of modulating synaptic weights as done in XdG, our algorithm sets the branch strength matrices of all DendSNNs in the network based on q . Mathematically, the modulation process can be described as

$$\{\mathbf{K}^{(n)}\}_{n=0}^{N-1} \leftarrow \text{DBG}(q) \quad (5)$$

where $\mathbf{K}^{(n)}$ denotes the branch strength matrix of the n -th DendSNN in the network, and N is the total number of DendSNNs. The remaining issue lies in mapping q to a set of N matrices with shape $T \times B$. The first approach, named $\text{DBG}_{\text{embedding}}$, assigns a set of dense but learnable matrices for each q . However, the density of $\text{DBG}_{\text{embedding}}$ deviates from the principle of synaptic clustering, which implies that the synaptic weights learned from a particular task should cluster on a small subset of dendritic branches. To achieve this goal, the $\text{DBG}(q)$ mapping should yield sparse and temporally homogeneous (i.e. all T rows being identical) matrices. In response, we propose two more strategies: DBG_{1hot} and $\text{DBG}_{\text{random}}$, both of which satisfy these requirements. For sparse DBG implementations like these, training-time modulation prevents the learning of a new task from updating all the weights learned on previous tasks. Inference-time gating, on the other hand, ensures the activation of the correct subnetwork for each task. These properties are crucial for successfully avoiding catastrophic forgetting. Refer to [Methods](#) for a detailed explanation of DBG and its implementation, and Supplementary Information S5 for pseudocodes.

To assess the task-incremental learning performance across different model types and modulation methods, we first use fully connected networks to solve the Permuted MNIST problem [69, 77] consisting of 50 tasks (Figure 4c). Figure 4d depicts the average accuracy curves concerning the number of learned tasks, where the descending trends reflect the impact of catastrophic forgetting on these models. Surprisingly, DendSNNs demonstrate greater resilience to catastrophic forgetting than point SNN, particularly in the early stages of incremental learning (i.e. less than 20 learned tasks), even without the assistance of DBG. As the number of learned tasks increases, DendSNNs with leaky ReLU and unlearnable Swish [78] activation functions consistently outperform point SNN, while that with non-monotonic Mexican hat activation exhibits inferior performance. Next, we focus on the Mexican hat activation function cases, since the effect of DBG is more pronounced under this setting. Figure 4f showcases the final average accuracies on 50 tasks. After DBG_{1hot} is applied, DendSNNs achieve significantly higher average accuracy compared to the baseline point SNN. The overall performance improves with an increase in the number of dendritic branches B , as fewer tasks are allocated to each branch as B increases; the performance of each task, however, does not dramatically degrade with the decrease in size of the subnetwork corresponding to the task, which is consistent with the observation in a previous study [79]. When B is set to 50 and DBG_{1hot} is adopted, the average accuracy even surpasses the best result point-SNN-based XdG [77] can achieve. Figure 4e plots the heat map of task i accuracy after learning task 0 to j (i for the row index and j for the column index), indicating that the test accuracies of previous tasks do not degrade after learning new tasks with DBG_{1hot} applied to a DendSNN with 50 branches. If we use DBG_{1hot} on a 5-branch DendSNN, the test accuracies of previous tasks do degrade, as each branch cannot

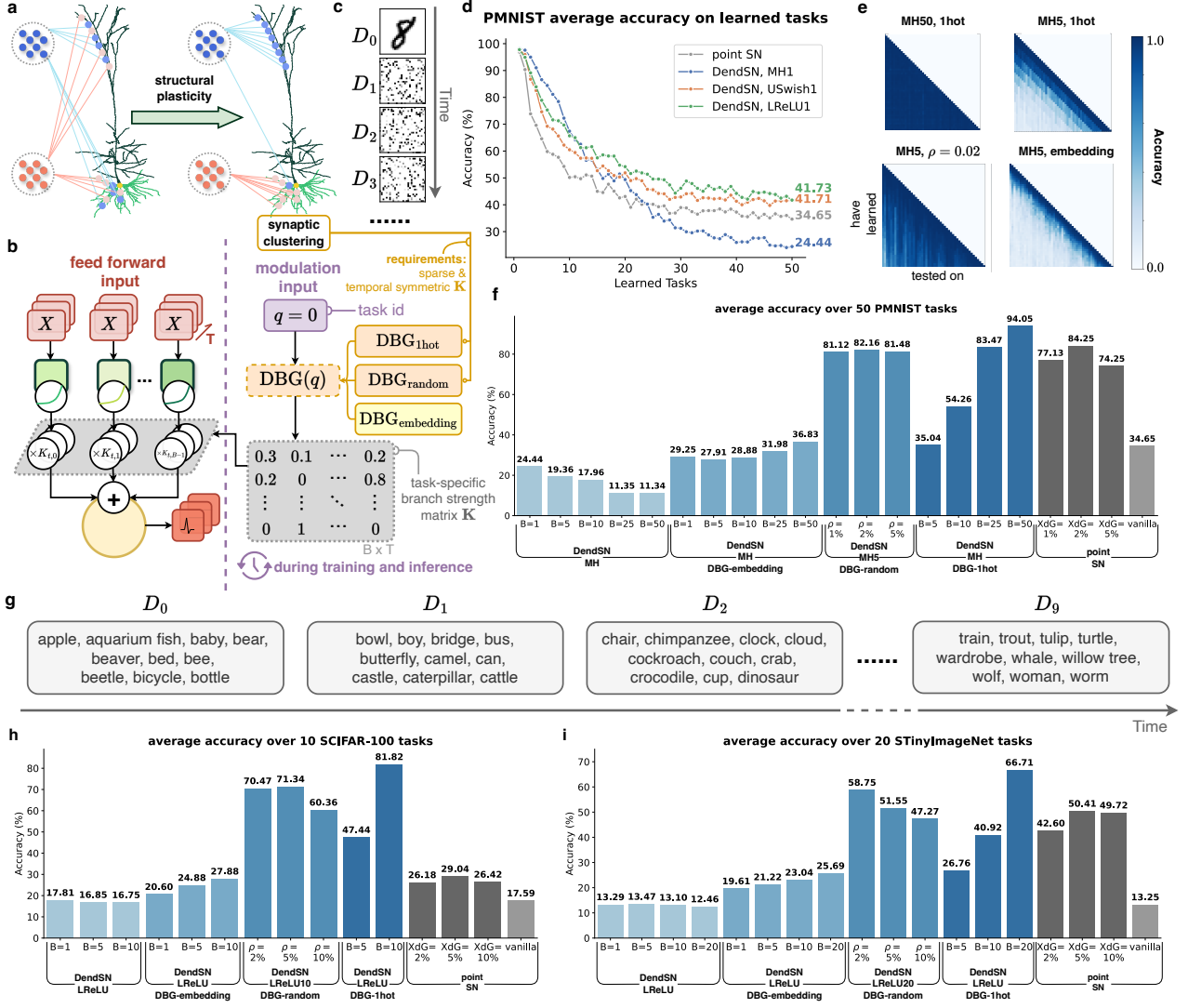


Figure 4 Dendritic branch gating (DBG) for mitigating catastrophic forgetting in task-incremental learning. **a)** An illustration of synaptic clustering in biological neurons. With the help of structural plasticity, functionally related synapses tend to cluster on dendrites, reducing interference from less relevant inputs. **b)** The DBG algorithm. During training and inference on task q , each DendSN in the network has its branch strength matrix $\mathbf{K}_{T \times B}$ set as a matrix that depends on the context signal q . This work proposes three implementations of DBG: $\text{DBG}_{1\text{hot}}$, $\text{DBG}_{\text{random}}$, and $\text{DBG}_{\text{embedding}}$. The first two implementations set \mathbf{K} as a sparse and temporally symmetric matrix, aligning with the synaptic clustering hypothesis. **c)** The Permuted MNIST tasks. In task D_q , all the samples are permuted using Perm_q . **d),e),f)** Results on the Permuted MNIST tasks. Subfigure e and f focus on DendSNNs with Mexican hat activation function to highlight the effect of DBG. **g)** The Split CIFAR-100 tasks. **h),i)** Results on the Split CIFAR-100 and Split TinyImageNet tasks.

afford to learn 10 tasks. $\text{DBG}_{\text{random}}$, on the other hand, enhances the models' continual learning performance, and even outperforms $\text{DBG}_{1\text{hot}}$ with $B \leq 10$, as Figure 4e and Figure 4f show. Their average accuracies are comparable to those of XdG on point SNNs. Conversely, if $\text{DBG}_{\text{embedding}}$ is applied, no significant improvement in average accuracy is observed compared with point SNN. Indeed, the performance is even worse than that of the baseline point SNN when $B \leq 25$. This underscores the importance of employing sparse gating in DBG and promotes synaptic clustering for achieving biological-inspired continual learning. For more information about the results, see Table S4.

We conduct further experiments on the Split CIFAR-100 [80] and Split TinyImageNet datasets (details are provided in Methods), where deeper convolutional networks (SEW ResNets [21]) are trained. We utilize DendSNNs with leaky ReLU dendritic activation instead of Mexican hat nonlinearity, since the latter one cannot scale up to deeper networks (see Supplementary Information S1). The task setting of Split CIFAR-100 is outlined in Figure 4g, with Split TinyImageNet following a similar structure. Figure 4h and Figure 4i show the average accuracies on the 10 Split CIFAR-100 tasks and 20 Split TinyImageNet tasks respectively. We observe similar trends to those observed in Permuted MNIST, with one notable exception: both vanilla DendSNNs with a small

B value and DendSNNs with $\text{DBG}_{\text{embedding}}$ outperform vanilla point SNNs. In addition, XdG yields intriguingly inferior performances on Split CIFAR-100. This phenomenon can be attributed to the fact that XdG zeros out most neuronal outputs, reducing the actual hidden size of each subnetwork and thereby impairing point SNNs’ capacity. Sparse DBG methods, nevertheless, do not significantly hurt DendSNNs’ capacity. For detailed experimental methodologies, refer to [Methods](#). It is worth noting that DBG can be applied to DendSNNs together with powerful replay-based [81], regularization-based [80, 82], and optimization-based [83] methods widely used in point neural networks to boost up the continual learning performance to an even higher level.

Apart from continual learning, DBG can be easily extended to multitask learning settings. The results of Multi-(Fashion+MNIST) [84] and UTKFace [85] multitask learning benchmarks are provided in Supplementary Information S7, where DendSNNs with some DBG conditions can obtain marginally better performance than point SNNs. In a nutshell, DBG provides a unified bio-inspired solution for task-context-aware learning, leading the deep learning community to exploit the inner structure of neurons for lifelong learning and multitask learning.

Performances on diverse machine learning scenarios

The exceptional task-context-aware learning performance of DendSNNs is propelled by a manually designed, although bio-inspired, algorithm. Additionally, we highlight the intrinsic advantages of the DendSN model for deep SNNs in this section.

Traditional ANNs and SNNs often falter when confronted with corrupted data, such as noisy inputs and adversarial attacks. They also encounter difficulties in few-shot learning scenarios, where training data are extremely scarce. By contrast, the human brain can handle all these challenges with ease, showcasing the remarkable robustness and generalization ability of biological neural circuits. We attribute this performance gap between artificial and biological systems to the disparities between real neural circuits and man-made models. To bridge this gap, a possible approach is to make artificial models more “brain-like”. We contend that the integration of dendritic computing into neural networks using DendSN has the potential to enhance performance and robustness in these challenging scenarios, even in the absence of specialized learning algorithms. We verify this hypothesis by conducting experiments on these scenarios, as listed in Figure 5a. We compare the performances of models using point SNNs or DendSNNs as the whole model or merely the backbone.

Noise robustness

Noise robustness is crucial for deep learning models to maintain stable and reliable performance in real-world situations where data are susceptible to diverse sources of noise or corruption. To assess DendSNNs’ robustness against noisy input, we conduct classification experiments on the FashionMNIST dataset [65] with varying levels of Gaussian noise infused (see Figure 5b). The models are first trained on either clean or noisy training sets, and then evaluated on the test sets with different noise levels. As shown in Figure 5c, with the increase in noise level, the classification accuracies of all the models decrease. Nonetheless, when trained on the clean training set, DendSNNs consistently outperform point SNNs across all noise levels, showing better noise robustness. Even when trained with noisy data, networks of 2-branch DendSNNs still achieve the best performances, exhibiting slower accuracy decrease rates than point SNNs. These findings suggest that multi-branch dendritic structures are beneficial for SNNs to resist noise.

However, Gaussian noise alone cannot cover the diverse corruption types in real life. To this end, we comprehensively test DendSNNs’ robustness against various noise types on CIFAR-10-C and TinyImageNet-C [86]. The networks are first trained on the clean training set and frozen after that. Then, their error rates are obtained on the corrupted validation set, which comprises multiple corruption types (20 for CIFAR-10-C and 15 for TinyImageNet-C), each with 5 levels of severity (see Figure 5d). We aggregate the models’ error rates across corruption types and severities using the mean corruption error (mCE) and relative mean corruption error (rmCE) metrics introduced by Hendrycks et al. [86] (see [Methods](#)), and report the results in Figure 5e and Figure 5f. On the CIFAR-10-C task, all DendSNNs show better robustness than the point SNN baseline (the pink dashed line) in terms of both mCE and rmCE. On TinyImageNet-C, which poses a greater challenge than the previous task, networks with 4-branch DendSN and leaky ReLU branch nonlinearity yield much lower rmCEs compared to the point SNN, while the mCE is slightly higher given lower test accuracies on the clean test set. Reducing the number of branches leads to a decrease in mCE (due to better performance on the clean test set) and an increase in rmCE (due to worse performance on the corrupted test set). From these observations, we can conclude that more dendritic branches are advantageous for noise robustness in sacrifice of clean accuracy.

In the aforementioned cases, noises are added to static images. We next investigate DendSNNs’ robustness against corruptions added to event streams. Similar to CIFAR-10-C and TinyImageNet-C, we construct a

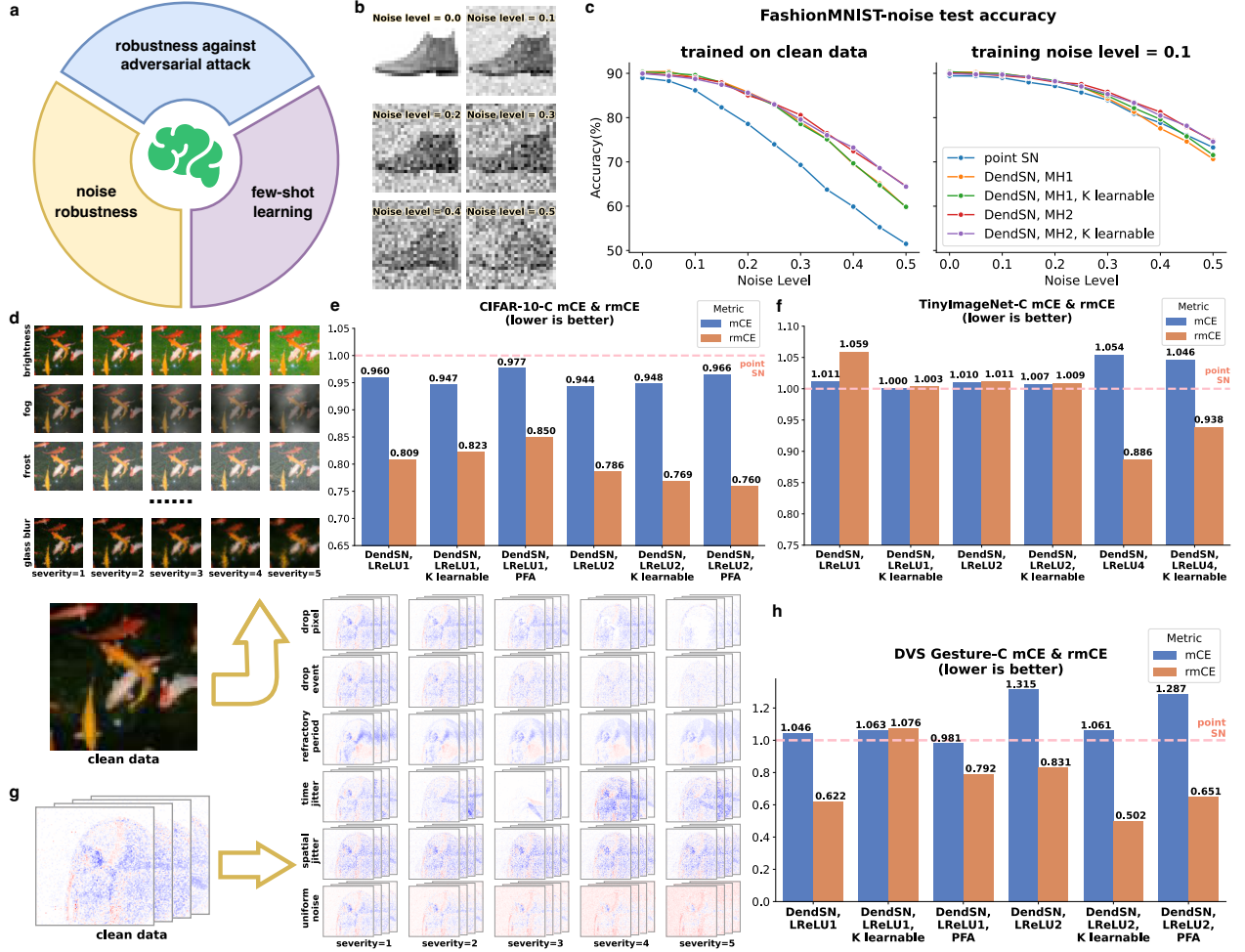


Figure 5 DendSNNs’ noise robustness. **a)** In this section, we are going to test the performance of DendSNNs on three challenging machine learning scenarios: noise robustness, robustness against adversarial attacks, and few-shot learning. **b)** Samples from the FashionMNIST dataset with different levels of Gaussian noise infused (FashionMNIST-noise). **c)** DendSNNs’ performances on FashionMNIST-noise. In the left plot, the model is trained on the clean training set and then tested on test sets with various noise levels. DendSNNs consistently outperform point SNNs. In the right plot, the model is trained on the noisy training set instead. Networks of DendSNNs with 2 branches achieve the best performances. **d)** An illustration of the TinyImageNet-C dataset. Corruptions are added to each sample in the validation set. There are 15 corruption types, each with 5 levels of severity. **e), f)** DendSNNs’ robustness on the CIFAR-10-C and TinyImageNet-C dataset. Their performances are compared with a point SNN (the pink dashed line), and mCE as well as rmCE are reported [86]. Lower mCE and rmCE are better. All the DendSNNs exhibit better robustness than the point SNN baseline on CIFAR-10-C, while on TinyImageNet-C, networks of DendSNNs with 4 branches achieve significantly lower rmCEs compared to point SNN. **g)** An illustration of the DVS Gesture-C dataset. Six types of corruptions, each with 5 severity levels, are applied to each sample in the test set. **h)** DendSNNs’ robustness on the DVS Gesture-C dataset. The baseline (the pink dashed line) is a point SNN. Five of the six DendSNNs achieve far lower rmCEs than point SNN.

corrupted version of the DVS Gesture dataset [87] by applying multiple types of corruptive transformations with different levels of severities to the events in the test set, as demonstrated in Figure 5g. The transformation pipeline is further introduced in Methods and Table S7. Experimental procedures mirror those of CIFAR-10-C, and the resulting mCEs and rmCEs are demonstrated in Figure 5h. Five of the six DendSNNs obtain significantly lower rmCEs and comparable mCEs compared to the baseline. Notice that a network of DendSNNs with 2 branches, leaky ReLU activation function and learnable branch strengths can even achieve a rmCE of 0.502 with a mCE of 1.061, indicating remarkable robustness and comparable clean accuracy. Taken together, these results support the hypothesis that DendSNNs are more robust against noise than point SNNs.

Robustness against adversarial attacks

Besides noise, adversarial attacks represent another form of data corruption obtained by applying tiny yet intentionally worst-case perturbations to original samples [88]. Enhancing the robustness of neural networks against adversarial attacks is critical for security concerns. Previous studies have shown that deep SNNs are

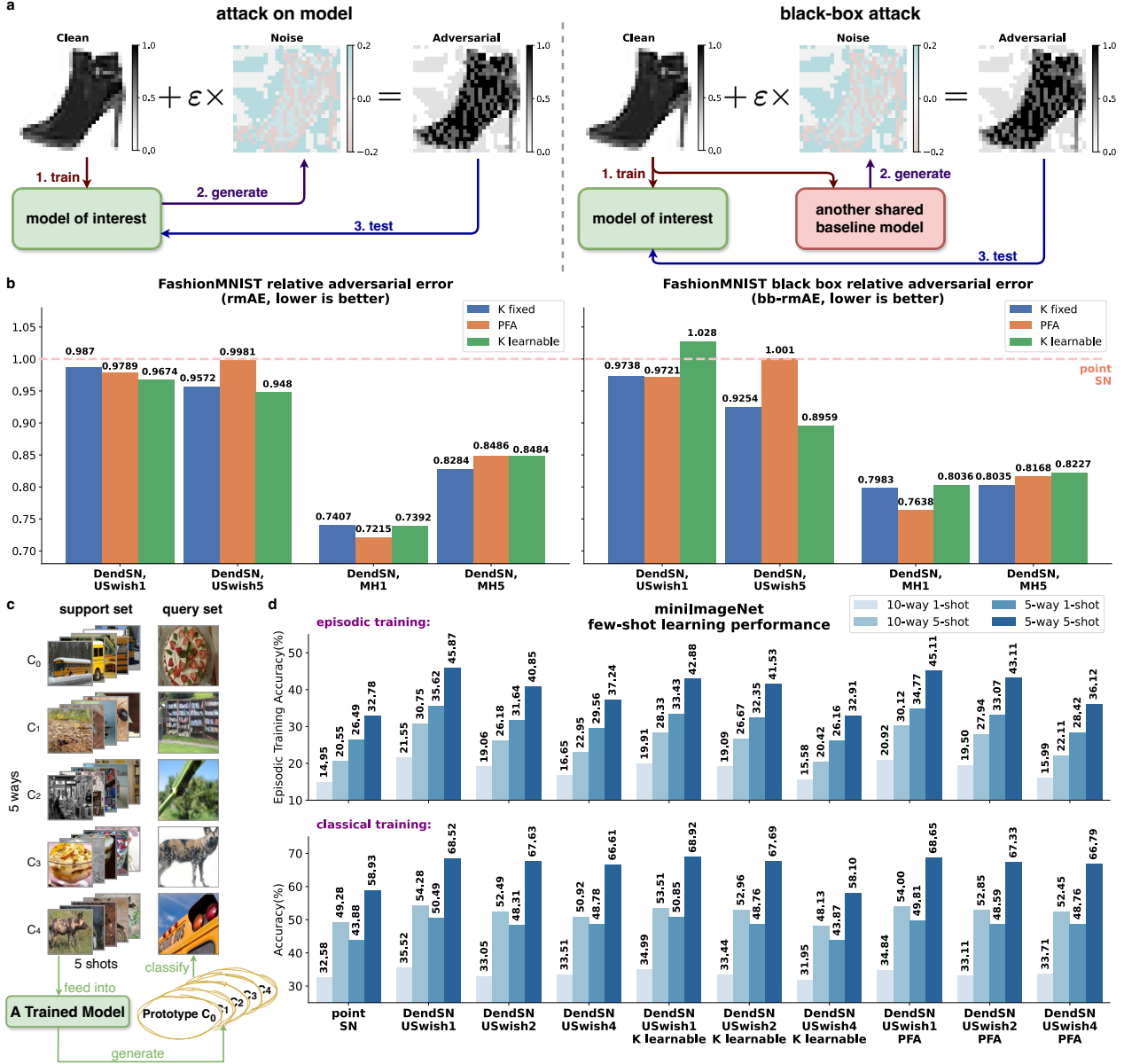


Figure 6 DendSNNs’ robustness against adversarial attack and few-shot learning performances. **a)** The procedures of the adversarial attack experiment. The left part depicts an “attack-on-model” setup, where adversarial attacks are applied directly to the model of interest. The right part, however, portrays a “black-box” scenario, where another shared baseline model is employed to generate the adversarial samples. **b)** DendSNNs’ robustness against adversarial attack, tested on the FashionMNIST benchmark. Their performances are compared to a point SNN with similar architecture (the pink dashed line). Lower rmAE indicates better robustness. In the left plot, attacks are applied directly to the models of interest, while in the right plot, attacks are applied to a shared baseline model. **c)** The procedures of few-shot learning using Prototypical Network. In each episode, there is a support set with multiple categories, each including several samples. These samples are processed by a trained feature extractor to generate one prototype for each category. These prototypes are then employed to classify the samples in the query set, using the nearest-neighbor principle. **d)** DendSNNs’ performances on the miniImageNet few-shot learning benchmark. The models are trained using either episodic training (top) or classical training (bottom) pipeline, and then evaluated using 5-way 1-shot, 5-way 5-shot, 10-way 1-shot, and 10-way 5-shot classification accuracies. DendSNNs obtain better results compared to point SNN.

inherently more robust against adversarial attacks compared to non-spiking ANNs [89, 90]. To check whether DendSNNs are less vulnerable to adversarial attacks than traditional SNNs, we conduct experiments based on the FashionMNIST dataset (the left part of Figure 6a). After training the models of interest on the original dataset, we employ the fast gradient sign method (FGSM) [88] to generate adversarial samples with respect to these models. The models’ error rates on both the original and adversarial test sets under various perturbation amplitudes ϵ are then recorded. Finally, we compute the relative mean adversarial error (rmAE), a metric similar to rmCE [86], as a summarized measure (refer to Methods). The left plot in Figure 6b compares rmAEs

of different models. Remarkably, 10 out of 12 DendSNN configurations achieve lower rmAEs than the point SNN baseline, suggesting better robustness against adversarial attacks. Mexican hat dendritic nonlinearity can further enhance the models’ resistance against attacks, and the network of DendSNNs with 1 branch and parameter-free attentive branch strength yields the lowest rmAE of 0.7215.

In the previous setup, adversarial attacks are applied directly to the models of interest. As a result, the test set for one model is different from another, leading to unfairness. To make the comparisons more reasonable, we next adopt a black-box adversarial attack setting, as shown in the right part of Figure 6a. This time, adversarial test samples are generated with regard to a shared baseline model whose architecture is different from all models of interest. All the other settings are identical to the previous case. Despite the black-box adjustment, the final results demonstrated in the right part of Figure 6b exhibit a trend similar to the previous setting. In summary, DendSNNs are more robust against adversarial attacks than point SNNs.

Few-shot learning

Conventionally, supervised training of deep neural networks relies heavily on a substantial amount of labeled training data. Obtaining so much labeled data, however, is often costly and time-consuming. Hence, it’s expected that machine learning models can effectively generalize to unseen domains and make accurate predictions when provided with very limited labeled training data. Here, we assess the few-shot learning capabilities of different backbone models using the miniImageNet benchmark [91]. We adopt the Prototypical Network paradigm [92] (Figure 6c), and choose SEW ResNet18 architecture [21] as the backbone for feature extraction due to its relatively high performance. Both episodic training [91] and classical training pipelines are constructed (see [Methods](#) for details), and the models are evaluated using 5-way 1-shot, 5-way 5-shot, 10-way 1-shot, and 10-way 5-shot classification accuracies. As shown in Figure 6d, all four types of accuracies under both episodic and classical training settings are elevated when a point SNN backbone is replaced with a DendSNN variant, regardless of the value of B and the configuration of dendritic branch strengths. These results indicate that multiple nonlinear dendritic branches can enhance the feature extractor’s robustness to variations in the input domain. DendSNNs are thus capable of extracting more generalizable features and distance metrics [92]. This insight offers potential solutions to alleviate the data-hungry bottleneck in various machine learning applications.

Discussions

The deep learning community has been dedicated to enhancing the performance of neural networks by designing novel functional modules and network architectures from a macroscopic perspective. The neurons in these networks, although acting as the fundamental computational and structural units, have not undergone sufficient exploration. The majority of existing deep ANNs and SNNs are built upon point neurons, which lack the microscopic morphology and nonlinear dynamics brought by dendrites and can not fully capture the expressivity of real biological neurons. Consequently, the expressivity of these networks is limited by the simplicity of their underlying neurons [27–30]. In this study, we propose the DendSN model, aiming to enrich the capacity of deep SNNs by incorporating dendritic computation into spiking neurons. The neuron model features both dendritic morphology and nonlinear dynamics, exhibiting significantly higher expressivity than point spiking neurons and possessing the ability to approximate the biophysical behavior of a detailed multi-compartment neuron in the subthreshold regime. Moreover, networks of DendSNNs can be trained through gradient-based learning rules and demonstrate superior supervised learning performance over point SNNs.

The endeavor to add structural and dynamical complexity to neurons in deep SNNs, however, is often accompanied by two streams of problems. Firstly, higher complexity usually results in unaffordable costs of memory and computation, hindering the application of such models to large-scale tasks and deep networks. Secondly, morphologically detailed neuron models are less flexible than point neurons, as their compatibility with complex network structures is limited. Most of the existing dendritic neuron models are tailored for specific network architectures, such as fully connected networks [49, 93]. Consequently, they have fewer opportunities to exploit the advantages of various deep network architectures. Our model tackles both problems with ingenuity. To reduce memory and computational load, we use a single compartment to represent a dendritic branch, neglecting further morphological details. We preserve only the passive dynamics on dendritic branches, while moving the active components to the dendrite-to-soma signal propagation process. This shift enables parallel dendritic computing across branch and time dimensions, speeding up neuronal simulation to a great extent. Compared to point spiking neurons, the extra computational overhead of DendSNNs is under controllable levels. Also, we use hand-crafted Triton kernels to customize DendSN layer’s low-level computational logic on GPUs so that the simulation efficiency can be further improved. As a result, we can build up and optimize DendSNNs

with depths and scales comparable to conventional SNNs. Moreover, DendSNNs are highly flexible, as they can be integrated into deep networks with nearly any architecture. Once organized into layers, DendSNNs can be placed after weight layers, receiving weighted features as raw inputs. These tensors are folded along the channel dimension, and each fold is assigned to a specific branch of all the neurons in the layer. Hierarchical networks featuring dendritic computation can then be built up following both DendSNN’s construction rule and those established design principles of deep learning. The computational efficiency and flexibility of DendSNNs lay a solid foundation for their practical application to deep learning.

Prior researches have extensively demonstrated the impact of dendritic morphology and dynamics on neuronal information processing using biophysical models of single neurons [39, 52, 53]. There have also been works that employed reduced phenomenological models to explore the dendritic contributions to circuit-level computation and functions [94]. However, in deep neural networks, the specific influence of dendrites on the optimization process or overall task performance has not been systematically investigated. To disentangle this issue, we assess the performance of DendSNNs in a variety of scenarios that are challenging for conventional SNNs. We first devised an innovative algorithm, DBG, to mimic the dendritic modulation mechanism and synaptic clustering phenomenon in biological neural circuits. DBG can effectively mediate catastrophic forgetting in task-incremental learning setups, and has the potential to be extended to other task-context-aware learning scenarios (e.g. multitask learning). In addition, our subsequent experiments revealed DendSNNs’ heightened robustness against noise and adversarial attacks, as well as improved generalization ability in few-shot learning scenarios. Our results suggest that DendSNNs might be more adept at handling complex real-world tasks than conventional point SNNs. This insight provides a compelling motivation for the integration of dendritic computing in deep SNNs.

In future works, we plan to adapt DendSNNs to deeper networks and tasks of larger scales (e.g. ImageNet classification [95]), aiming to narrow the gap between DendSNNs and state-of-the-art deep network models. To achieve this, we recognize the urgent need for refined network structures and specially tailored training methodologies. We will also persistently explore the applicability of DendSNNs across diverse real-world task scenarios, extending beyond the confines of image classification. Potential areas of research include brain-machine interfaces, which demand low energy consumption along with model expressivity and robustness. What’s more, we intend to further enhance the biological feasibility of DendSNNs by devising alternative approaches to incorporate dendritic nonlinearity while maintaining low computational cost, and by developing biologically plausible learning rules leveraging dendritic states and properties for effective training of deep networks. These pursuits align with our goal of advancing DendSNNs beyond traditional simulations, making DendSNNs valuable tools for designing and implementing brain-like models and learning rules on deep neural networks. For a more detailed discussion about the limitations of the current work and our future research directions, refer to Supplementary Information S10.

In summary, our work opens a promising avenue for integrating dendritic computing into practical deep SNNs for machine learning, extending the applicability of these models beyond computational neuroscience simulations.

Methods

Dendritic spiking neuron model

A dendritic spiking neuron (DendSN) comprises B segregated dendritic branches and one soma. Each dendritic branch $i \in \{0, \dots, B-1\}$ is depicted by a single compartment with local potential v_i^d , governed by the leaky integrator dynamics with time constant τ_d , resting state v_{rest} , and input $x_i(t)$.

$$\tau_d \frac{dv_i^d}{dt} = -(v_i^d - v_{\text{rest}}^d) + x_i(t) \quad (6)$$

For efficient computational implementation, we assume $v_{\text{rest}}^d = 0$ and adopt the following discrete form.

$$\begin{aligned} V_i^d[0] &= X_i[0] \\ V_i^d[t] &= \alpha V_i^d[t-1] + X_i[t] \end{aligned} \quad (7)$$

Here, $t \in \{0, \dots, T-1\}$ is the time step, $0 \leq \alpha < 1$ is the decay factor depending on τ_d , while $V_i^d[t]$ and $X_i[t]$ correspond to $v_i^d(t)$ and $x_i(t)$ in Equation (6), respectively. Specifically, $X_i[t]$ is the input to dendritic branch i at time step t , whose value is the weighted sum of the pre-synaptic spikes $\{S_j^{\text{pre}}[t]\}_{j=0}^{J-1}$. Take fully connected

(FC) architecture as an example,

$$X_i[t] = \sum_{j=0}^{J-1} W_{ij} S_j^{\text{pre}}[t] \quad (8)$$

where W_{ij} is the weight from pre-synaptic neuron j to dendritic branch i .

At the joint of dendritic branch i and the soma, V_i^d is activated and weighted, yielding the branch-to-soma signal Y_i according to

$$Y_i[t] = K_{t,i} f_i(V_i^d[t]) \quad (9)$$

where $\mathbf{K} = [K_{t,i}]_{T \times B}$ is the dendritic branch strength matrix (further illustrated in subsection “[Dendritic branch strength](#)”), and f_i is the nonlinear dendritic activation function at branch i . Notably, $\mathcal{F} = \{f_i\}_{i=0}^{B-1}$ can add different nonlinear properties to different branches, acting as the source of dendritic heterogeneity [48] that has been proven to be crucial for the remarkable computational capacity of dendritic neurons. In our study, we explore four choices for \mathcal{F} : non-monotonic Mexican hat function (MH), monotonically increasing leaky ReLU (LReLU), Swish function with trainable slope parameter for each branch (Swish) [78], and Swish function with randomly initialized but fixed slope parameter (USwish, “U” for “unlearnable”). Notice that the first two situations assign the same function to all the branches, as special cases of our formulation. See Supplementary Information S1 for more details about dendritic branch nonlinearity.

The soma is a leaky integrate-and-fire (LIF) neuron, obeying

$$\begin{aligned} \tau_s \frac{dv^s}{dt} &= -(v^s - v_{\text{rest}}^s) + \sum_i y_i(t) \\ \lim_{t \rightarrow t_f^+} v^s(t) &= v_{\text{reset}}^s \\ t_f &\in \{t \mid v(t) = v_{\text{th}}^s\} \end{aligned} \quad (10)$$

Assuming $v_{\text{rest}}^s = 0$, $v_{\text{reset}}^s = 0$ and $v_{\text{th}}^s = 1$, the discrete form is

$$\begin{aligned} H^s[t] &= \beta V^s[t-1] + (1-\beta) \sum_{i=0}^{B-1} Y_i[t] \\ S[t] &= \Theta(H^s[t] - V_{\text{th}}^s) \\ &= \Theta(H^s[t] - 1) \\ V^s[t] &= (1 - S[t])H^s[t] + S[t]V_{\text{reset}}^s \\ &= (1 - S[t])H^s[t] \end{aligned} \quad (11)$$

Here, $0 \leq \beta < 1$ is the decay factor depending on τ_s , $H^s[t]$ is the somatic membrane potential before spike emission, Θ is the Heaviside step function, V_{th}^s is the firing threshold, and V_{reset}^s is the somatic reset potential. For conditions adopting an integrate-and-fire (IF) soma, the update of H^s obeys the following equation instead.

$$H^s[t] = V^s[t-1] + \sum_{i=0}^{B-1} Y_i[t] \quad (12)$$

Viewing the neuron as a whole, an individual DendSN maps the weighted sum of pre-synaptic spikes (i.e. \mathbf{X}) to somatic spikes (i.e. \mathbf{S}). Equations (7), (9), and (11) can be summarized as

$$\begin{aligned} \mathbf{X} &\triangleq \{X_i[t] \mid t \in \{0, \dots, T-1\}, i \in \{0, \dots, B-1\}\} \\ \mathbf{S} &\triangleq \{S[t] \mid t \in \{0, \dots, T-1\}, S[t] \in \{0, 1\}\} \\ \mathbf{S} &= \text{DendSN}(\mathbf{X}; \alpha, \mathbf{K}, \mathcal{F}, \beta) \end{aligned} \quad (13)$$

For the neuronal parameter settings used in our experiments, see Table S9.

Acceleration of dendritic state update

Equation (7) describes the dynamics of dendritic local potential $\{V_i^d\}_{i=0}^{B-1}$. Notice that the dendritic state on one branch $V_{i_1}^d$ is totally independent of that on another branch $V_{i_2}^d$ ($i_1 \neq i_2$), since the branches are parallel

and electrically segregated in our assumption. Therefore, the states on different branches can be updated in parallel.

In addition, since $V_i^d[0] = X_i[0]$, Equation (7) can be rewritten as

$$V_i^d[t] = \sum_{\tau=0}^t \alpha^{t-\tau} X_i[\tau] \quad (14)$$

Let $\vec{V}_i^d = (V_i^d[0], \dots, V_i^d[T-1])$ and $\vec{X}_i = (X_i[0], \dots, X_i[T-1])$. Using this notation, we can express the relationship as

$$\vec{V}_i^d = \mathbf{A} \vec{X}_i^T \quad (15)$$

Here, \mathbf{A} is a lower triangular coefficient matrix, with each element defined as $A_{i,j} = 1_{i \geq j} \cdot \alpha^{i-j}$. \mathbf{A} can be computed in advance and reused if T is fixed (a common situation in deep SNNs). This formulation allows for the efficient calculation of dendritic states at each time step through a matrix-vector multiplication, enabling parallel processing across time steps. PyTorch code for implementing a DendSN layer with or without this acceleration technique is offered in Supplementary Information S2.

Dendritic spiking neural networks

To incorporate DendSNNs into SNNs, we have to organize them into layers. Analogous to point spiking neuron layers in conventional SNNs, DendSN layers are positioned after weight layers, acting as activation functions.

For simplicity, each dendritic neuron in the layer is constrained to have the same number of dendritic branches B . Other neuronal parameters $\alpha, \beta, \mathcal{F}$ are also shared, while \mathbf{K} is not necessarily the same across neurons. As implied by the shape of \mathbf{X} and \mathbf{S} in Equation (13), a DendSN layer will compress the features to $1/B$ of the original shape, deviating from the practice of point neuron layers that keep the shape unchanged. This feature compression process should be applied along the channel dimension in order to fuse information from different channels at each location. Specifically, let $\tilde{\mathbf{X}}[t] \in \mathbb{R}^{C_0 \times \dots}$ represent the output tensor of the previous weight layer at time step t , where $C_0 = c_0 B$ is the number of channels (feature maps), and the ellipsis here stands for spatial dimensions. For instance, $\tilde{\mathbf{X}}[t] \in \mathbb{R}^{C_0}$ for fully connected layers, and $\tilde{\mathbf{X}}[t] \in \mathbb{R}^{C_0 \times H \times W}$ for 2D convolutional layers. These C_0 feature maps are divided into B groups using modular arithmetic, and the i -th group is fed to the i -th dendritic branch of all the neurons.

$$\mathbf{X}_i^{(c, \dots)}[t] = \tilde{\mathbf{X}}^{(cB+i, \dots)}[t] \quad (16)$$

where $i \in \{0, \dots, B-1\}$, $c \in \{0, \dots, c_0-1\}$, $t \in \{0, \dots, T-1\}$. Here, $\mathbf{X}_i^{(c, \dots)}$ is the input to the i -th dendritic branch of all the neurons at channel c , while $\tilde{\mathbf{X}}^{(cB+i, \dots)}$ is the $(cB+i)$ -th feature map of $\tilde{\mathbf{X}}$. Consequently, the dendritic neurons in this layer form an array with shape (c_0, \dots) , and emit an output spike tensor of that shape at each time step. PyTorch implementations of a DendSN layer are given in Supplementary Information S2, providing a possible implementation of this feature assignment rule.

By concatenating multiple weight-DendSN blocks, deep dendritic spiking neural networks (DendSNNs) of arbitrary architecture can be constructed, mirroring the flexibility of convolutional deep SNN structure. These networks can be directly trained using spatio-temporal backpropagation (STBP) [64] and surrogate gradient [62]. We also rewrite DendSN dynamics as Triton kernels, aiming to customize the underlying parallel computation and compile our program into highly efficient GPU code. The flexibility and computational efficiency of DendSNNs ensure the scalability of DendSNNs to large-scale tasks.

Dendritic branch strength

The dendritic branch strength matrix $\mathbf{K} \in \mathbb{R}^{T \times B}$ in Equation (9) controls the weights of dendrite-to-soma signals at each time step. This subsection delves into the strategies to generate $\{\mathbf{K}^{(n)}\}_{n=0}^{N-1}$ for all the N DendSNNs in a layer, where $\mathbf{K}^{(n)} \in \mathbb{R}^{T \times B}$ denotes the strength matrix of the n -th DendSN. By **default**, $\mathbf{K}^{(n)}$ is an all-ones matrix ($K_{t,i}^{(n)} = 1, \forall t, i$) and is fixed throughout training. To enhance the model's performance, we explore three approaches: learning $\{\mathbf{K}^{(n)}\}_{n=0}^{N-1}$ directly, employing multi-dimensional attention (MDA), and implementing parameter-free attention (PFA).

Learning $\{\mathbf{K}^{(n)}\}_{n=0}^{N-1}$ directly: $\{\mathbf{K}^{(n)}\}_{n=0}^{N-1}$ serves as dendrite-soma connection weights. Therefore, they can be directly trained using STBP [64] together with other learnable parameters in the network. Similar to the default case, $\mathbf{K}^{(n)}$ is initialized as $\mathbf{1}_{T \times B}$. To reduce the number of extra learnable parameters, we impose

a constraint that all the DendSNs in the layer share the same weight matrix during training $\mathbf{K}^{(n)} = \mathbf{K}, \forall n$. For simplicity, the learning rate and optimizer are the same as those of other learnable parameters. Making $\{\mathbf{K}^{(n)}\}_{n=0}^{N-1}$ learnable enhances DendSNN’s capacity, introducing merely $T \times B$ extra learnable parameters for each DendSN layer (often negligible compared to the number of synaptic weights). Also, it can be easily implemented using popular deep learning frameworks. We widely use this strategy in our experiments.

Multi-dimensional attention: Viewing dendritic branch strengths as attention weights over temporal and branch dimensions, we introduce a multi-dimensional attention (MDA) mechanism inspired by MA-SNN [96]. MDA employs the CBAM channel attention module [66] sequentially along temporal and branch dimensions, extracting $\mathbf{K}^{(n)}$ from the activated dendrite-to-soma signal $\tilde{\mathbf{Y}}^{(n)} \in \mathbb{R}^{T \times B}$, where $\tilde{Y}_{t,i}^{(n)} = f(V_i^d[t])$.

$$\begin{aligned}
g_t(\tilde{\mathbf{Y}}^{(n)}) &= \sigma(\text{MLP}_t(\text{AvgPool}(\tilde{\mathbf{Y}}^{(n)}, \text{dim} = 1)) \\
&\quad + \text{MLP}_t(\text{MaxPool}(\tilde{\mathbf{Y}}^{(n)}, \text{dim} = 1))) \\
\tilde{\mathbf{Y}}_{\text{TA}}^{(n)} &= g_t(\tilde{\mathbf{Y}}^{(n)}) \odot \tilde{\mathbf{Y}}^{(n)} \\
g_b(\tilde{\mathbf{Y}}_{\text{TA}}^{(n)}) &= \sigma(\text{MLP}_b(\text{AvgPool}(\tilde{\mathbf{Y}}_{\text{TA}}^{(n)}, \text{dim} = 0)) \\
&\quad + \text{MLP}_b(\text{MaxPool}(\tilde{\mathbf{Y}}_{\text{TA}}^{(n)}, \text{dim} = 0))) \\
\mathbf{K}^{(n)} &= g_t(\tilde{\mathbf{Y}}^{(n)}) \odot g_b(\tilde{\mathbf{Y}}_{\text{TA}}^{(n)})
\end{aligned} \tag{17}$$

Here, $\text{AvgPool}(\cdot, \text{dim} = d)$ denotes average pooling along dimension d while retaining the matrix’s shape (by filling the average value into all the elements of the pooled dimension), while $\text{MaxPool}(\cdot, \text{dim} = d)$ stands for max pooling. MLP_t and MLP_b are MLPs projecting along the temporal and branch dimensions, respectively. The hidden size and output size of MLP_t are both T , while those of MLP_b are B . \odot denotes element-wise multiplication, and $\sigma(\cdot)$ is the sigmoid function. MDA is designed to capture the temporal and branch-wise importance of the dendritic signals. It introduces only $T^2 + B^2$ extra parameters for each DendSN layer. It is beneficial in situations where T and B are large. However, in practical DendSNN applications, T and B are usually small due to memory constraints. Our experience is that MDA tends to reduce DendSNNs’ performance in such cases, and it also introduces huge extra computational overhead. Therefore, we employ MDA only in the FashionMNIST supervised learning experiments. Developers should use MDA with caution.

Parameter-free attention: To avoid introducing extra parameters (i.e. MLP_t and MLP_b in Equation (17)), we propose a parameter-free attention (PFA) mechanism inspired by SimAM [67]. PFA dynamically derive $\mathbf{K}^{(n)}$ from $\tilde{\mathbf{Y}}^{(n)}$ through operations outlined in Equation (18).

$$\begin{aligned}
M &= T \times B - 1 \\
\hat{\mu}^{(n)} &= \text{MEAN}(\tilde{\mathbf{Y}}^{(n)}) \\
\widehat{\text{var}}^{(n)} &= \frac{1}{M} \sum_{t,i} (\tilde{Y}_{t,i}^{(n)} - \hat{\mu}^{(n)})^2 \\
K_{t,i}^{(n)} &= \sigma \left[\frac{(\tilde{Y}_{t,i}^{(n)} - \hat{\mu}^{(n)})^2 + 2\widehat{\text{var}}^{(n)} + 2\lambda}{4(\widehat{\text{var}}^{(n)} + \lambda)} \right]
\end{aligned} \tag{18}$$

Here, λ is a regularization hyperparameter, typically set to 10^{-4} . According to Yang et. al., this formulation attaches attention weights to dendritic branches based on the distinctiveness of their activity patterns [67]. Compared to MDA, PFA is lightweight and easy to implement. We find that PFA works well in DendSNNs with small T and B , where MDA tends to fail. This drives us to use PFA in most of our experiments.

Dendritic branch gating

Inspired by dendritic modulation mechanism [55] and synaptic clustering phenomenon [56, 57] in neuroscience, we design a new algorithm named dendritic branch gating (DBG) to utilize task context signals for better performances in task-context-aware learning scenarios like task-incremental learning and multitask learning. The main idea is to modulate the dendritic branch strength matrices of all the DendSNs in a network using the index of the current task. Here, we follow the notation in the previous section and discuss how to generate $\{\mathbf{K}^{(n)}\}_{n=0}^{N-1}$ for a layer of N DendSNs using DBG.

Suppose a DendSNN is going to learn Q tasks indexed $q \in \{0, \dots, Q-1\}$. For continual learning setups, these tasks are sequentially presented (e.g. those described in subsection “[Details of continual learning experiments](#)”);

for multitask learning setups, they are presented simultaneously. The index q is called the task context signal and is fed into the network as a top-down modulation input together with the bottom-up feedforward input. Note that the use of an extra task context signal is a common practice in previous works like XdG [77]. DBG assigns a set of task-specific branch strength matrices to each DendSN layer using a mapping $\text{DBG} : \{0, \dots, Q-1\} \rightarrow \mathbb{R}^{N \times T \times B}$. During both training and inference on task q , the strength matrices in the layer are set as $\text{DBG}(q)$. Pseudocodes for this process are given in Supplementary Information S5.

In this study, we propose three implementations of the mapping $\text{DBG}(q)$. The most trivial one is $\text{DBG}_{\text{embedding}}$, which produces dense but learnable strength matrices for each task q . It is called “embedding” due to its similarity to the learnable word embedding technique in natural language processing. The embedding matrices are optimized using STBP alongside other learnable parameters in the model.

To bring the principle of synaptic clustering into the design of DBG, we propose two more implementations: DBG_{1hot} and $\text{DBG}_{\text{random}}$. Both of them generate sparse and temporally symmetric (all rows being identical) strength matrices for each task so as to cluster the weights for each task on a small subset of branches. DBG_{1hot} encodes q using one-hot vectors.

$$\text{DBG}_{\text{1hot}}(q) = \{\mathbf{K}_{\text{1hot},q}^{(n)}\}_{n=0}^{N-1} \quad \text{where :} \quad \mathbf{K}_{\text{1hot},q}^{(n)} = \begin{bmatrix} \mathbf{e}_{(q \bmod B)} \\ \vdots \\ \mathbf{e}_{(q \bmod B)} \end{bmatrix}_{T \times B}, \quad \forall n \quad (19)$$

where \mathbf{e}_i is a one-hot vector with the i -th element being 1 and other elements being 0. $\text{DBG}_{\text{random}}$ randomly generates strength values and binary masks for each task.

$$\text{DBG}_{\text{random}}(q) = \{\mathbf{K}_{\text{random},q}^{(n)}\}_{n=0}^{N-1} \quad \text{where :} \quad \mathbf{K}_{\text{random},q}^{(n)} = \begin{bmatrix} \text{Normalize}(\mathbf{m}_q^{(n)} \odot \mathbf{v}_q^{(n)}) \\ \vdots \\ \text{Normalize}(\mathbf{m}_q^{(n)} \odot \mathbf{v}_q^{(n)}) \end{bmatrix}_{T \times B}, \quad \forall n \quad (20)$$

Here, $\mathbf{m}_q^{(n)}$ is a random binary mask vector with length B , whose elements are sampled from the Bernoulli distribution with parameter ρ . $\mathbf{v}_q^{(n)}$ is a vector with each of the B elements drawn from the standard normal distribution. $\text{Normalize}(\cdot)$ normalizes the vector so that it sums to 0 (if all the elements are zero) or 1 (otherwise). $\text{Normalize}(\cdot)$ is implemented by applying softmax on non-zero elements of each row.

Details of the simulating efficiency experiment

We compare the computational overhead of three neuron models: a LIF neuron (point SN), a DendSN whose dendritic dynamics are simulated in parallel across both time steps and branches (DendSN Parallel), and a DendSN whose dendritic dynamics are simulated in sequence along time steps while in parallel across branches (DendSN Vanilla). In each trial, the neurons are simulated for T discrete time steps. The input to the DendSNs at each time step is a real-valued vector of length B drawn from the standard normal distribution, whose elements are fed to the B dendritic branches correspondingly. By contrast, the input to the LIF neuron is a real random scalar at each time step. We simulate the models for 512 trials and use total time cost as the metric for comparison. This process is repeated for different values of T and B , whose ranges are displayed in Figure 2c. The neuron models are implemented in PyTorch [61] and simulated on a single Nvidia GeForce RTX 2080Ti GPU.

Details of L5PC data approximation

Beniaguev et al. constructed a detailed multi-compartment model of a layer 5 pyramidal cell (L5PC) from a rat’s brain, and collected electrophysiological data by simulating the model [30]. We try to predict the somatic membrane potential of the L5PC model given the presynaptic spikes, using a point LIF neuron or a DendSN. First, the spike train data are binned into 6000 discrete time steps (1ms for each time step). Each sample is then cropped so that it contains only the first $T = 2048$ time steps. A total of $C = 1278$ channels of presynaptic spikes are recorded, with half representing the excitatory components and the other half representing the inhibitory components at the corresponding synaptic sites. Among the $1278/2 = 639$ synapses, 377 are located at the apical dendrite, yielding $C_{\text{apical}} = 754$ apical channels. The other $C_{\text{basal}} = 524$ channels come from 262

synaptic sites on the basal dendrite. The dataset is split into training, validation, and test sets with a ratio of 8 : 1 : 1.

In this experiment, we use DendSNs with $B = 2$ dendritic branches to model the apical and basal dendrites of the L5PC neuron. The input spikes are weighted by synaptic connections, fed forward into their corresponding dendritic branches, and finally integrated according to DendSN’s dynamics. For the point neuron case, however, the presynaptic spikes are weighted, summed, and directly fed into the soma at each time step. We use the mean squared error (MSE) between the somatic membrane potential of our models and that of the L5PC model as the loss, and optimize the synaptic weights as well as branch strength values (for DendSNs) using gradient descent. Notably, the degree of freedom of DendSNs’ \mathbf{K} is sometimes restricted as directed by the experimental condition. We select the models’ versions with the lowest loss on the validation set and evaluate them on the test set. Test losses are treated as the metric for comparison. The detailed hyperparameter settings are provided in Table S8.

Details of supervised learning experiments

FashionMNIST [65] is a more challenging variant of MNIST task [97], whose goal is to classify grey-scale images of size 28×28 items into 10 categories. In FashionMNIST supervised learning experiments, we use a fully connected architecture with $\text{FC}(784 \rightarrow 2000) \Rightarrow \text{NL}_1 \Rightarrow \text{FC}(2000/B \rightarrow 2000B) \Rightarrow \text{NL}_2 \Rightarrow \text{FC}(2000 \rightarrow 10)$, where NL_1 and NL_2 are point or dendritic neuron layers, and B is the number of dendritic branches (for point neuron layers, assume $B = 1$). The fully connected layers have no bias terms, so the total number of learnable parameters does not change with hyperparameter B . We let $T = 4$. At each time step, the pixel values are fed directly to the network as input, and the first weight-DendSN block serves as a learnable spike encoder. The output spike train is summed along the temporal dimension, yielding the output logits; this is equivalent to adding an IF point neuron layer with an infinite firing threshold after the last FC layer, and taking the membrane potential at the last time step as the output [98]. We use softmax cross-entropy loss and the Adam optimizer with default parameter settings [99]. For a detailed hyperparameter setting, see Table S8.

N-MNIST is an event-based digit recognition dataset captured by Asynchronous Time-based Image Sensor (ATIS) through saccadic movements [68]. It contains 10 classes of handwritten digits. To enable supervised training using a deep learning framework, we first convert each event stream into T frames of size 34×34 using Fang et al.’s method [32]. The frames are then fed to the network time step by time step. Here, we use a simple network with two convolution-DendSN blocks, followed by a fully connected layer as the classifier. The convolutional layers have 32 and $32B$ kernels respectively, all of which are of size 3×3 . The training settings resemble that of the FashionMNIST experiment. Refer to Table S8 for a detailed hyperparameter setting.

Details of continual learning experiments

We denote a continual learning scenario as $\{D_q\}_{q=0}^{Q-1}$, where D_q is the q -th task. A model should be trained on these tasks sequentially, using a supervised learning setting similar to that described in subsection “[Details of supervised learning experiments](#)”. Additional algorithms (e.g. DBG and XdG [77]) might be applied to facilitate continual learning, according to each experimental condition. To evaluate the models’ resistance to catastrophic forgetting, we use the average accuracy as the metric

$$\overline{acc}_q = \frac{\sum_{j=0}^q acc_{qj}}{q+1}, \quad q \in \{0, \dots, Q-1\} \quad (21)$$

where acc_{qj} is the accuracy of the model on task j after sequentially trained on task 0 to q .

The Permuted MNIST [69, 77] experiment consists of $Q = 50$ image classification tasks, each of which is a different pixel-level permutation of the entire original MNIST task [97] (i.e. all the samples in the original dataset are permuted using Perm_q). An illustration is provided in Figure 4c. We adopt 50 random seeds to generate the permutations, and all experimental conditions share the same set of seeds. We use the same network architecture as that in the FashionMNIST experiment. Hyperparameter configurations are listed in Table S8.

The Split CIFAR-100 [80] divides the CIFAR-100 dataset [100] into $Q = 10$ subsets (or tasks) $\{D_0, \dots, D_9\}$. We formulate each task as a 10-way classification problem, and D_q contains all the samples of category $10q$ to $10q + 9$ in the original dataset (see Figure 4g). We adopt a network architecture similar to Zheng et al.’s SpikingResNet17 [20], but substitute SEW blocks [21] for spiking residual blocks and enlarge the number of channels in each Conv2d layer. Also, we use a weight-neuron block instead of a 2-layer MLP as the classification

head, and treat the membrane potential of the infinite-threshold neurons at the last time step as the final output. Refer to Table S8 for a detailed hyperparameter setting.

The Split TinyImageNet experiment resembles Split CIFAR-100. The original dataset is split into $Q = 20$ subsets, each as a 10-way classification task. The network architecture follows the design of SEW ResNet18 [21], but we make modifications on the classification head similar to what we have done in the Split CIFAR-100 experiment. Table S8 lists the hyperparameter setting.

Details of noise robustness experiments

In the FashionMNIST-noise experiment, we add standard Gaussian noise with 11 levels of amplitude 0, 0.05, 0.10, \dots , 0.50 on the test set, and induce 2 levels of noise 0, 0.10 on the training set. First, on the training set with noise level l_{train} , we train a network with the same architecture as that in the FashionMNIST experiment. After that, we evaluate its accuracy on the test set with noise level l_{test} . $2 \times 11 = 22$ combinations of l_{train} and l_{test} are obtained. Hyperparameter settings are listed in Table S8. We use test accuracies to evaluate the model’s noise robustness.

CIFAR-10-C, TinyImageNet-C, and DVS Gesture-C are three corruption robustness benchmarks containing test samples with various types and levels of corruptions. The corrupted CIFAR-10-C and TinyImageNet-C test sets are given by Hendrycks et al. [86], while the DVS Gesture-C test set is generated by ourselves based on the DVS Gesture event-based dataset [87] using the Tonic API [101] (summarized in Table S7). We employ a network structure similar to the one used in the Split CIFAR100 experiment for CIFAR-10-C (but with fewer channels), a Spike-driven Transformer [25] for TinyImageNet-C, and a modified 7B-Net [21] architecture (replacing max pooling with average pooling, LIF with IF) for DVS Gesture-C. In all these corruption robustness experiments, the SNNs are first trained on clean training sets and then evaluated on the noisy test sets with different corruption types and severities. We use the mean corruption errors (mCEs) and relative mean corruption errors (rmCEs) [86] as the metrics for these two experiments.

$$\begin{aligned} \text{mCE}^f &= \text{MEAN}_c \left[\frac{\sum_s (1 - \text{acc}_{s,c}^f)}{\sum_s (1 - \text{acc}_{s,c}^{\text{point}})} \right] \\ \text{rmCE}^f &= \text{MEAN}_c \left[\frac{\sum_s (\text{acc}_{\text{clean}}^f - \text{acc}_{s,c}^f)}{\sum_s (\text{acc}_{\text{clean}}^{\text{point}} - \text{acc}_{s,c}^{\text{point}})} \right] \end{aligned} \quad (22)$$

where f is the model of interest, $\text{acc}_{s,c}^f$ is the accuracy of f on the test set with corruption type c and severity s , $\text{acc}_{\text{clean}}^f$ is the accuracy of f on the clean test set, and point refers to the point SNN. For hyperparameter settings, see Table S8.

Details of adversarial attack experiments

The networks for FashionMNIST adversarial attack experiments share the same architecture as that in the FashionMNIST supervised training experiment. Firstly, they are optimized on the clean training set and evaluated on the clean test set. Then, we generate adversarial test samples with respect to these models using the fast gradient sign method (FGSM) [88] under different perturbation amplitudes $\epsilon \in \{0.00, 0.04, \dots, 0.20\}$. Similar to the noise robustness experiments, we calculate the relative mean adversarial error (rmAE) as the metric

$$\text{rmAE}^f = \text{MEAN}_\epsilon \left(\frac{\text{acc}_{\text{clean}}^f - \text{acc}_\epsilon^f}{\text{acc}_{\text{clean}}^{\text{point}} - \text{acc}_\epsilon^{\text{point}}} \right) \quad (23)$$

where f is the model of interest, $\text{acc}_{\text{clean}}^f$ is the accuracy of f on the clean test set, acc_ϵ^f is the accuracy of f on the adversarial test set with perturbation amplitude ϵ , and point refers to the point SNN. Here, we treat ϵ like c in Equation (22) instead of s so as to ensure a more objective comparison.

For the “black-box attack” case, we train another baseline ANN with 3 Conv2d layers and one FC layer on the FashionMNIST training set. FGSM with different perturbation levels is applied to generate adversarial samples with respect to this ANN. These samples are fed to all the models of interest for evaluation, and black-box rmAEs are computed according to Equation (23).

Details of few-shot learning experiments

The miniImageNet benchmark [91] for few-shot learning consists of 60,000 images (84×84 resolution) of 100 different categories. Among these categories, 60 classes are used for training, 16 for validation, and 20 for testing. We use a SEW ResNet18 [21] architecture as the feature extractor, and construct a prototypical network [92] on its basis. In **classical training** cases, we train the feature extractor together with a fully connected classification head directly on the entire training set, just like the supervised learning setting. For each N -way K -shot task during inference (see Figure 6c), we use the trained feature extractor to extract features, compute one prototype for each of the N classes using the support set, and classify the query set using the nearest-neighbor rule. In **episodic training** cases, a N -way K -shot task is randomly sampled from the training set, and the feature extractor is optimized together with a classification head using a N -class cross-entropy loss. The inference time procedure is identical to the classical case. We report 5-way 1-shot, 5-way 5-shot, 10-way 1-shot, and 10-way 5-shot classification accuracies as the metrics. Hyperparameters are listed in Table S8.

Data availability

All data used in this paper are publicly available and can be accessed via the following links:

- L5PC data: https://github.com/SelfishGene/neuron_as_deep_net
- FashionMNIST: <https://github.com/zalandoresearch/fashion-mnist>
- N-MNIST: <https://www.garrickorchard.com/datasets/n-mnist>
- MNIST (for Permuted MNIST): <http://yann.lecun.com/exdb/mnist/>
- CIFAR-100 (for Split CIFAR-100) and CIFAR-10 (as CIFAR-10-C training set): <https://www.cs.toronto.edu/~kriz/cifar.html>
- TinyImageNet (for Split TinyImageNet, and as TinyImageNet-C training set): <http://cs231n.stanford.edu/tiny-imagenet-200.zip>
- CIFAR-10-C and TinyImageNet-C test sets: <https://github.com/hendrycks/robustness>
- DVS Gesture (for DVS Gesture-C): <https://research.ibm.com/interactive/dvsgesture/>
- miniImageNet (split specification files, csv): <https://github.com/yaoyao-liu/mini-imagenet-tools>. The image data are from ImageNet 2012: <https://www.image-net.org/challenges/LSVRC/2012/>
- Multi-(Fashion+MNIST): <https://github.com/Xi-L/ParetoMTL/tree/master/multiMNIST/data>
- UTKFace: <https://susanqq.github.io/UTKFace/>

Code availability

A readable PyTorch implementation of DendSN is given in Supplementary Information S2. A detailed implementation of DendSN and the experiment codes will be publicly available at <https://github.com/AllenYolk/dendsn-experiments> once the paper is accepted and published (currently, the repository is private).

References

- [1] Alex Krizhevsky, Ilya Sutskever, and Geoffrey E. Hinton. Imagenet classification with deep convolutional neural networks. *Commun. ACM*, 60(6):84–90, 2017.
- [2] Kaiming He, Xiangyu Zhang, Shaoqing Ren, and Jian Sun. Deep residual learning for image recognition. In *Proceedings of the IEEE Conference on Computer Vision and Pattern Recognition (CVPR)*, pages 770–778, 2016.
- [3] Ashish Vaswani, Noam Shazeer, Niki Parmar, Jakob Uszkoreit, Llion Jones, Aidan N. Gomez, Łukasz Kaiser, and Illia Polosukhin. Attention is all you need. In *Advances in Neural Information Processing Systems*, volume 30, pages 5998–6008, 2017.
- [4] Jacob Devlin, Ming-Wei Chang, Kenton Lee, and Kristina Toutanova. BERT: Pre-training of deep bidirectional transformers for language understanding. In *Proceedings of the 2019 Conference of the North American Chapter of the Association for Computational Linguistics: Human Language Technologies*, volume 1, pages 4171–4186, 2019.
- [5] OpenAI. Gpt-4 technical report, 2024.

- [6] Mathias Lechner, Ramin Hasani, Alexander Amini, Thomas A. Henzinger, Daniela Rus, and Radu Grosu. Neural circuit policies enabling auditable autonomy. *Nature Machine Intelligence*, 2(10):642–652, 2020.
- [7] Charles Vorbach, Ramin Hasani, Alexander Amini, Mathias Lechner, and Daniela Rus. Causal navigation by continuous-time neural networks. In *Advances in Neural Information Processing Systems*, volume 34, pages 12425–12440, 2021.
- [8] Adam Coates, Brody Huval, Tao Wang, David Wu, Bryan Catanzaro, and Ng Andrew. Deep learning with cots hpc systems. In *Proceedings of the 30th International Conference on Machine Learning*, volume 28, pages 1337–1345, Atlanta, Georgia, USA, 2013.
- [9] Sharan Chetlur, Cliff Woolley, Philippe Vandermersch, Jonathan Cohen, John Tran, Bryan Catanzaro, and Evan Shelhamer. cudnn: Efficient primitives for deep learning, 2014.
- [10] Zhe Jia, Marco Maggioni, Jeffrey Smith, and Daniele Paolo Scarpazza. Dissecting the nvidia turing t4 gpu via microbenchmarking, 2019.
- [11] Demis Hassabis, Dhharshan Kumaran, Christopher Summerfield, and Matthew Botvinick. Neuroscience-inspired artificial intelligence. *Neuron*, 95(2):245–258, 2017.
- [12] Kaushik Roy, Akhilesh Jaiswal, and Priyadarshini Panda. Towards spike-based machine intelligence with neuromorphic computing. *Nature*, 575(7784):607–617, 2019.
- [13] Mike Davies, Narayan Srinivasa, Tsung-Han Lin, Gautham Chinya, Yongqiang Cao, Sri Harsha Choday, Georgios Dimou, Prasad Joshi, Nabil Imam, Shweta Jain, Yuyun Liao, Chit-Kwan Lin, Andrew Lines, Ruokun Liu, Deepak Mathaikutty, Steven McCoy, Arnab Paul, Jonathan Tse, Guruguhanathan Venkataramanan, Yi-Hsin Weng, Andreas Wild, Yoonseok Yang, and Hong Wang. Loihi: A neuromorphic manycore processor with on-chip learning. *IEEE Micro*, 38(1):82–99, 2018.
- [14] Michael V. DeBole, Brian Taba, Arnon Amir, Filipp Akopyan, Alexander Andreopoulos, William P. Risk, Jeff Kunitz, Carlos Ortega Otero, Tapan K. Nayak, Rathinakumar Appuswamy, Peter J. Carlson, Andrew S. Cassidy, Pallab Datta, Steven K. Esser, Guillaume J. Garreau, Kevin L. Holland, Scott Lekuch, Michael Mastro, Jeff McKinstry, Carmelo di Nolfo, Brent Paulovicks, Jun Sawada, Kai Schleupen, Benjamin G. Shaw, Jennifer L. Klamo, Myron D. Flickner, John V. Arthur, and Dharmendra S. Modha. Truenorth: Accelerating from zero to 64 million neurons in 10 years. *Computer*, 52(5):20–29, 2019.
- [15] Jing Pei, Lei Deng, Sen Song, Mingguo Zhao, Youhui Zhang, Shuang Wu, Guanrui Wang, Zhe Zou, Zhenzhi Wu, Wei He, et al. Towards artificial general intelligence with hybrid tianjic chip architecture. *Nature*, 572(7767):106–111, 2019.
- [16] Hananel Hazan, Daniel J. Saunders, Hassaan Khan, Devdhar Patel, Darpan T. Sanghavi, Hava T. Siegelmann, and Robert Kozma. Bindsnet: A machine learning-oriented spiking neural networks library in python. *Frontiers in Neuroinformatics*, 12, 2018.
- [17] Jason K. Eshraghian, Max Ward, Emre O. Neftci, Xinxin Wang, Gregor Lenz, Girish Dwivedi, Mohammed Bennamoun, Doo Seok Jeong, and Wei D. Lu. Training spiking neural networks using lessons from deep learning. *Proceedings of the IEEE*, 111(9):1016–1054, 2023.
- [18] Wei Fang, Yanqi Chen, Jianhao Ding, Zhaofer Yu, Timothée Masquelier, Ding Chen, Liwei Huang, Huihui Zhou, Guoqi Li, and Yonghong Tian. Spikingjelly: An open-source machine learning infrastructure platform for spike-based intelligence. *Science Advances*, 9(40):eadi1480, 2023.
- [19] Wolfgang Maass. Networks of spiking neurons: The third generation of neural network models. *Neural Networks*, 10(9):1659–1671, 1997.
- [20] Hanle Zheng, Yujie Wu, Lei Deng, Yifan Hu, and Guoqi Li. Going deeper with directly-trained larger spiking neural networks. *Proceedings of the AAAI Conference on Artificial Intelligence*, 35(12):11062–11070, 2021.

- [21] Wei Fang, Zhaofei Yu, Yanqi Chen, Tiejun Huang, Timothée Masquelier, and Yonghong Tian. Deep residual learning in spiking neural networks. In *Advances in Neural Information Processing Systems*, volume 34, pages 21056–21069, 2021.
- [22] Yifan Hu, Lei Deng, Yujie Wu, Man Yao, and Guoqi Li. Advancing spiking neural networks toward deep residual learning. *IEEE Transactions on Neural Networks and Learning Systems*, pages 1–15, 2024.
- [23] Zhaokun Zhou, Yuesheng Zhu, Chao He, Yaowei Wang, Shuicheng YAN, Yonghong Tian, and Li Yuan. Spikformer: When spiking neural network meets transformer. In *The Eleventh International Conference on Learning Representations*, 2023.
- [24] Chenlin Zhou, Liutao Yu, Zhaokun Zhou, Zhengyu Ma, Han Zhang, Huihui Zhou, and Yonghong Tian. Spikingformer: Spike-driven residual learning for transformer-based spiking neural network, 2023.
- [25] Man Yao, JiaKui Hu, Zhaokun Zhou, Li Yuan, Yonghong Tian, Bo Xu, and Guoqi Li. Spike-driven transformer. In *Advances in Neural Information Processing Systems*, volume 36, pages 64043–64058, 2023.
- [26] Man Yao, JiaKui Hu, Tianxiang Hu, Yifan Xu, Zhaokun Zhou, Yonghong Tian, Bo XU, and Guoqi Li. Spike-driven transformer v2: Meta spiking neural network architecture inspiring the design of next-generation neuromorphic chips. In *The Twelfth International Conference on Learning Representations*, 2024.
- [27] Panayiota Poirazi, Terrence Brannon, and Bartlett W. Mel. Pyramidal neuron as two-layer neural network. *Neuron*, 37(6):989–999, 2003.
- [28] Monika P. Jädi, Bardia F. Behabadi, Alon Polog-Polsky, Jackie Schiller, and Bartlett W. Mel. An augmented two-layer model captures nonlinear analog spatial integration effects in pyramidal neuron dendrites. *Proceedings of the IEEE*, 102(5):782–798, 2014.
- [29] Alexandra Tzivilaki, George Kastellakis, and Panayiota Poirazi. Challenging the point neuron dogma: Fs basket cells as 2-stage nonlinear integrators. *Nature communications*, 10(1):3664, 2019.
- [30] David Beniaguev, Idan Segev, and Michael London. Single cortical neurons as deep artificial neural networks. *Neuron*, 109(17):2727–2739, 2021.
- [31] Louis Lapicque. Recherches quantitatives sur l’excitation électrique des nerfs traitée comme une polarisation. *Journal de Physiologie et de Pathologie Générale*, 9:620–635, 1907.
- [32] Wei Fang, Zhaofei Yu, Yanqi Chen, Timothée Masquelier, Tiejun Huang, and Yonghong Tian. Incorporating learnable membrane time constant to enhance learning of spiking neural networks. In *Proceedings of the IEEE/CVF International Conference on Computer Vision (ICCV)*, pages 2661–2671, 2021.
- [33] Christoph Stöckl and Wolfgang Maass. Optimized spiking neurons can classify images with high accuracy through temporal coding with two spikes. *Nature Machine Intelligence*, 3(3):230–238, 2021.
- [34] Frank Rosenblatt. The perceptron: a probabilistic model for information storage and organization in the brain. *Psychological review*, 65(6):386–408, 1958.
- [35] Michael L. Hines and Nicholas T. Carnevale. Neuron: A tool for neuroscientists. *The Neuroscientist*, 7(2):123–135, 2001.
- [36] Marcel Stimberg, Romain Brette, and Dan F. M. Goodman. Brian 2, an intuitive and efficient neural simulator. *eLife*, 8:e47314, 2019.
- [37] Panayiota Poirazi, Terrence Brannon, and Bartlett W. Mel. Arithmetic of subthreshold synaptic summation in a model cal pyramidal cell. *Neuron*, 37(6):977–987, 2003.
- [38] Erik De Schutter and James M. Bower. An active membrane model of the cerebellar purkinje cell. i. simulation of current clamps in slice. *Journal of Neurophysiology*, 71(1):375–400, 1994. PMID: 7512629.

- [39] Etay Hay, Sean L. Hill, Felix Schürmann, Henry Markram, and Idan Segev. Models of neocortical layer 5b pyramidal cells capturing a wide range of dendritic and perisomatic active properties. *PLoS Computational Biology*, 7(7):e1002107, 2011.
- [40] Michael London and Michael Häusser. Dendritic computation. *Annual Review of Neuroscience*, 28(2005):503–532, 2005.
- [41] Alexandre Payeur, Jean-Claude Béique, and Richard Naud. Classes of dendritic information processing. *Current Opinion in Neurobiology*, 58:78–85, 2019. Computational Neuroscience.
- [42] Jyotibdhya Acharya, Arindam Basu, Robert Legenstein, Thomas Limbacher, Panayiota Poirazi, and Xundong Wu. Dendritic computing: branching deeper into machine learning. *Neuroscience*, 489:275–289, 2022.
- [43] Ulisses Marti Mengual, Willem A.M. Wybo, Lotte J.E. Spierenburg, Mirko Santello, Walter Senn, and Thomas Nevian. Efficient low-pass dendro-somatic coupling in the apical dendrite of layer 5 pyramidal neurons in the anterior cingulate cortex. *Journal of Neuroscience*, 40(46):8799–8815, 2020.
- [44] Guy Major, Matthew E. Larkum, and Jackie Schiller. Active properties of neocortical pyramidal neuron dendrites. *Annual Review of Neuroscience*, 36(Volume 36, 2013):1–24, 2013.
- [45] Jordan Guerguiev, Timothy P. Lillicrap, and Blake A. Richards. Towards deep learning with segregated dendrites. *eLife*, 6:e22901, 2017.
- [46] João Sacramento, Rui Ponte Costa, Yoshua Bengio, and Walter Senn. Dendritic cortical microcircuits approximate the backpropagation algorithm. In *Advances in Neural Information Processing Systems*, volume 31, page 12, 2018.
- [47] Alexandre Payeur, Jordan Guerguiev, Friedemann Zenke, Blake A. Richards, and Richard Naud. Burst-dependent synaptic plasticity can coordinate learning in hierarchical circuits. *Nature Neuroscience*, 24(7):1010–1019, 2021.
- [48] Hanle Zheng, Zhong Zheng, Rui Hu, Bo Xiao, Yujie Wu, Fangwen Yu, Xue Liu, Guoqi Li, and Lei Deng. Temporal dendritic heterogeneity incorporated with spiking neural networks for learning multi-timescale dynamics. *Nature Communications*, 15(1):277, 2024.
- [49] Xundong Wu, Xiangwen Liu, Wei Li, and Qing Wu. Improved expressivity through dendritic neural networks. In *Advances in Neural Information Processing Systems*, volume 31, 2018.
- [50] Abhiram Iyer, Karan Grewal, Akash Velu, Lucas Oliveira Souza, Jeremy Forest, and Subutai Ahmad. Avoiding catastrophe: Active dendrites enable multi-task learning in dynamic environments. *Frontiers in Neurorobotics*, 16:846219, 2022.
- [51] Mariana-Iuliana Georgescu, Radu Tudor Ionescu, Nicolae-Cătălin Ristea, and Nicu Sebe. Nonlinear neurons with human-like apical dendrite activations. *Applied Intelligence*, 53(21):25984–26007, 2023.
- [52] Songting Li, Nan Liu, Xiaohui Zhang, David W. McLaughlin, Douglas Zhou, and David Cai. Dendritic computations captured by an effective point neuron model. *Proceedings of the National Academy of Sciences*, 116(30):15244–15252, 2019.
- [53] Brendan A. Bicknell and Michael Häusser. A synaptic learning rule for exploiting nonlinear dendritic computation. *Neuron*, 109(24):4001–4017, 2021.
- [54] Philippe Tillet, H. T. Kung, and David Cox. Triton: an intermediate language and compiler for tiled neural network computations. In *Proceedings of the 3rd ACM SIGPLAN International Workshop on Machine Learning and Programming Languages*, page 10–19. Association for Computing Machinery, 2019.
- [55] Willem A. M. Wybo, Matthias C. Tsai, Viet Anh Khoa Tran, Bernd Illing, Jakob Jordan, Abigail Morrison, and Walter Senn. Nmda-driven dendritic modulation enables multitask representation learning in hierarchical sensory processing pathways. *Proceedings of the National Academy of Sciences*, 120(32):e2300558120, 2023.

2023.

- [56] Joseph Cichon and Wen-Biao Gan. Branch-specific dendritic ca^{2+} spikes cause persistent synaptic plasticity. *Nature*, 520(7546):180–185, 2015.
- [57] Thomas Limbacher and Robert Legenstein. Emergence of stable synaptic clusters on dendrites through synaptic rewiring. *Frontiers in Computational Neuroscience*, 14, 2020.
- [58] Yichen Zhang, Gan He, Lei Ma, Xiaofei Liu, JJ Johannes Hjorth, Alexander Kozlov, Yutao He, Shenjian Zhang, Jeanette Hellgren Kotaleski, Yonghong Tian, et al. A gpu-based computational framework that bridges neuron simulation and artificial intelligence. *Nature Communications*, 14(1):5798, 2023.
- [59] Santiago Ramón y Cajal. *Estructura de los centros nerviosos de las aves*. 1888.
- [60] Norio Ishizuka, W. Maxwell Cowan, and David G. Amaral. A quantitative analysis of the dendritic organization of pyramidal cells in the rat hippocampus. *Journal of Comparative Neurology*, 362(1):17–45, 1995.
- [61] Adam Paszke, Sam Gross, Francisco Massa, Adam Lerer, James Bradbury, Gregory Chanan, Trevor Killeen, Zeming Lin, Natalia Gimelshein, Luca Antiga, Alban Desmaison, Andreas Kopf, Edward Yang, Zachary DeVito, Martin Raison, Alykhan Tejani, Sasank Chilamkurthy, Benoit Steiner, Lu Fang, Junjie Bai, and Soumith Chintala. Pytorch: An imperative style, high-performance deep learning library. In *Advances in Neural Information Processing Systems*, volume 32, 2019.
- [62] Emre O. Neftci, Hesham Mostafa, and Friedemann Zenke. Surrogate gradient learning in spiking neural networks: Bringing the power of gradient-based optimization to spiking neural networks. *IEEE Signal Processing Magazine*, 36(6):51–63, 2019.
- [63] Friedemann Zenke and Tim P Vogels. The remarkable robustness of surrogate gradient learning for instilling complex function in spiking neural networks. *Neural computation*, 33(4):899–925, 2021.
- [64] Yujie Wu, Lei Deng, Guoqi Li, Jun Zhu, and Luping Shi. Spatio-temporal backpropagation for training high-performance spiking neural networks. *Frontiers in Neuroscience*, 12:331, 2018.
- [65] Han Xiao, Kashif Rasul, and Roland Vollgraf. Fashion-mnist: a novel image dataset for benchmarking machine learning algorithms, 2017.
- [66] Sanghyun Woo, Jongchan Park, Joon-Young Lee, and In So Kweon. Cbam: Convolutional block attention module. In *Proceedings of the European Conference on Computer Vision (ECCV)*, pages 3–19, 2018.
- [67] Lingxiao Yang, Ru-Yuan Zhang, Lida Li, and Xiaohua Xie. Simam: A simple, parameter-free attention module for convolutional neural networks. In *Proceedings of the 38th International Conference on Machine Learning*, volume 139, pages 11863–11874, 2021.
- [68] Garrick Orchard, Ajinkya Jayawant, Gregory K. Cohen, and Nitish Thakor. Converting static image datasets to spiking neuromorphic datasets using saccades. *Frontiers in Neuroscience*, 9, 2015.
- [69] Ian J. Goodfellow, Mehdi Mirza, Da Xiao, Aaron Courville, and Yoshua Bengio. An empirical investigation of catastrophic forgetting in gradient-based neural networks, 2015.
- [70] Morgane M. Roth, Johannes C. Dahmen, Dylan R. Muir, Fabia Imhof, Francisco J. Martini, and Sonja B. Hofer. Thalamic nuclei convey diverse contextual information to layer 1 of visual cortex. *Nature neuroscience*, 19(2):299–307, 2016.
- [71] Serin Atiani, Mounya Elhilali, Stephen V. David, Jonathan B. Fritz, and Shihab A. Shamma. Task difficulty and performance induce diverse adaptive patterns in gain and shape of primary auditory cortical receptive fields. *Neuron*, 61(3):467–480, 2009.
- [72] Dina V. Popovkina and Anitha Pasupathy. Task context modulates feature-selective responses in area v4. *Journal of Neuroscience*, 42(33):6408–6423, 2022.

- [73] Bartlett W. Mel. Information processing in dendritic trees. *Neural Computation*, 6(6):1031–1085, 1994.
- [74] Jacopo Bono, Katharina A. Wilmes, and Claudia Clopath. Modelling plasticity in dendrites: from single cells to networks. *Current Opinion in Neurobiology*, 46:136–141, 2017. Computational Neuroscience.
- [75] George Kastellakis, Denise J. Cai, Sara C. Mednick, Alcino J. Silva, and Panayiota Poirazi. Synaptic clustering within dendrites: An emerging theory of memory formation. *Progress in Neurobiology*, 126:19–35, 2015.
- [76] Naoya Takahashi, Kazuo Kitamura, Naoki Matsuo, Mark Mayford, Masanobu Kano, Norio Matsuki, and Yuji Ikegaya. Locally synchronized synaptic inputs. *Science*, 335(6066):353–356, 2012.
- [77] Nicolas Y. Masse, Gregory D. Grant, and David J. Freedman. Alleviating catastrophic forgetting using context-dependent gating and synaptic stabilization. *Proceedings of the National Academy of Sciences*, 115(44):E10467–E10475, 2018.
- [78] Prajit Ramachandran, Barret Zoph, and Quoc V. Le. Searching for activation functions, 2017.
- [79] Youngeun Kim, Yuhang Li, Hyungseob Park, Yeshwanth Venkatesha, Ruokai Yin, and Priyadarshini Panda. Exploring lottery ticket hypothesis in spiking neural networks. In *European Conference on Computer Vision (ECCV)*, page 102–120, 2022.
- [80] Friedemann Zenke, Ben Poole, and Surya Ganguli. Continual learning through synaptic intelligence. In *Proceedings of the 34th International Conference on Machine Learning*, volume 70, pages 3987–3995, 2017.
- [81] Hanul Shin, Jung Kwon Lee, Jaehong Kim, and Jiwon Kim. Continual learning with deep generative replay. In *Advances in Neural Information Processing Systems*, volume 30, pages 2990–2999, 2017.
- [82] James Kirkpatrick, Razvan Pascanu, Neil Rabinowitz, Joel Veness, Guillaume Desjardins, Andrei A. Rusu, Kieran Milan, John Quan, Tiago Ramalho, Agnieszka Grabska-Barwinska, Demis Hassabis, Claudia Clopath, Dharshan Kumaran, and Raia Hadsell. Overcoming catastrophic forgetting in neural networks. *Proceedings of the National Academy of Sciences*, 114(13):3521–3526, 2017.
- [83] Mehrdad Farajtabar, Navid Azizan, Alex Mott, and Ang Li. Orthogonal gradient descent for continual learning. In *Proceedings of the Twenty Third International Conference on Artificial Intelligence and Statistics*, volume 108, pages 3762–3773, 2020.
- [84] Xi Lin, Hui-Ling Zhen, Zhenhua Li, Qing-Fu Zhang, and Sam Kwong. Pareto multi-task learning. In *Advances in Neural Information Processing Systems*, volume 32, 2019.
- [85] Zhifei Zhang, Yang Song, and Hairong Qi. Age progression/regression by conditional adversarial autoencoder. In *Proceedings of the IEEE Conference on Computer Vision and Pattern Recognition (CVPR)*, pages 4352–4360, 2017.
- [86] Dan Hendrycks and Thomas Dietterich. Benchmarking neural network robustness to common corruptions and perturbations, 2019.
- [87] Arnon Amir, Brian Taba, David Berg, Timothy Melano, Jeffrey McKinstry, Carmelo Di Nolfo, Tapan Nayak, Alexander Andreopoulos, Guillaume Garreau, Marcela Mendoza, Jeff Kusnitz, Michael Debole, Steve Esser, Tobi Delbruck, Myron Flickner, and Dharmendra Modha. A low power, fully event-based gesture recognition system. In *Proceedings of the IEEE Conference on Computer Vision and Pattern Recognition (CVPR)*, pages 7388–7397, 2017.
- [88] Ian J. Goodfellow, Jonathon Shlens, and Christian Szegedy. Explaining and harnessing adversarial examples, 2015.
- [89] Saima Sharmin, Priyadarshini Panda, Syed Shakib Sarwar, Chankyu Lee, Wachirawit Ponghiran, and Kaushik Roy. A comprehensive analysis on adversarial robustness of spiking neural networks. In *2019 International Joint Conference on Neural Networks (IJCNN)*, pages 1–8, 2019.

- [90] Saima Sharmin, Nitin Rathi, Priyadarshini Panda, and Kaushik Roy. Inherent adversarial robustness of deep spiking neural networks: Effects of discrete input encoding and non-linear activations. In *European Conference on Computer Vision (ECCV)*, page 399–414, 2020.
- [91] Oriol Vinyals, Charles Blundell, Timothy Lillicrap, koray kavukcuoglu, and Daan Wierstra. Matching networks for one shot learning. In *Advances in Neural Information Processing Systems*, volume 29, 2016.
- [92] Jake Snell, Kevin Swersky, and Richard Zemel. Prototypical networks for few-shot learning. In *Advances in Neural Information Processing Systems*, volume 30, 2017.
- [93] Yifei Yang, Mingkun Xu, Jing Pei, Peng Li, Guoqi Li, Si Wu, and Huanglong Li. Bio-realistic and versatile artificial dendrites made of anti-ambipolar transistors, 2022.
- [94] Michalis Pagkalos, Spyridon Chavlis, and Panayiota Poirazi. Introducing the dendrify framework for incorporating dendrites to spiking neural networks. *Nature Communications*, 14(1):131, 2023.
- [95] Jia Deng, Wei Dong, Richard Socher, Li-Jia Li, Kai Li, and Li Fei-Fei. Imagenet: A large-scale hierarchical image database. In *2009 IEEE Conference on Computer Vision and Pattern Recognition*, pages 248–255, 2009.
- [96] Man Yao, Guangshe Zhao, Hengyu Zhang, Yifan Hu, Lei Deng, Yonghong Tian, Bo Xu, and Guoqi Li. Attention spiking neural networks. *IEEE Transactions on Pattern Analysis and Machine Intelligence*, 45(8):9393–9410, 2023.
- [97] Yann Lecun, Leon Bottou, Yoshua Bengio, and Patrick Haffner. Gradient-based learning applied to document recognition. *Proceedings of the IEEE*, 86(11):2278–2324, 1998.
- [98] Chankyu Lee, Syed Shakib Sarwar, Priyadarshini Panda, Gopalakrishnan Srinivasan, and Kaushik Roy. Enabling spike-based backpropagation for training deep neural network architectures. *Frontiers in Neuroscience*, 14, 2020.
- [99] Diederik P. Kingma and Jimmy Ba. Adam: A method for stochastic optimization, 2017.
- [100] Alex Krizhevsky. Learning multiple layers of features from tiny images. 2009.
- [101] Gregor Lenz, Kenneth Chaney, Sumit Bam Shrestha, Omar Oubari, Serge Picaud, and Guido Zarrella. Tonic: event-based datasets and transformations., 2021.

Acknowledgments

We gratefully acknowledge Di Shang for advice on the continual learning experiments, and Kexin Wang, Yuhong Chou and Qiaoyi Su for the valuable discussions.

Author contributions

Y.T. supervised the whole project and led the writing of this paper. G.L. proposed the research direction, designed the overall structure of this paper, revised its contents, and supervised the progress of the experiments. Y.H. proposed the initial idea, carried out the experiments, and wrote the paper. W.F. revised the code and paper content, and proposed the acceleration strategy. Z.M. revised the structure and content of the paper.

Competing interests

The authors declare no competing interests.

Additional information

Supplementary information

Supplementary information is available at the end of this document.

Correspondence

Correspondence and requests for materials should be addressed to Guoqi Li and Yonghong Tian.

Supplementary Information For

Flexible and Scalable Deep Dendritic Spiking Neural Networks with Multiple Nonlinear Branching

Contents

S1	Dendritic branch activation functions	2
S2	PyTorch implementations of a DendSN layer	4
S3	Dense weights v.s. sparse weights in dendritic neural networks	6
S4	Supervised learning results	7
S5	Pseudocodes of dendritic branch gating	8
S6	Permuted MNIST continual learning results	10
S7	Multitask learning	11
S8	DVS Gesture-C dataset	14
S9	Hyperparameter settings for the experiments	15
S10	Limitations and future directions	16

S1 Dendritic branch activation functions

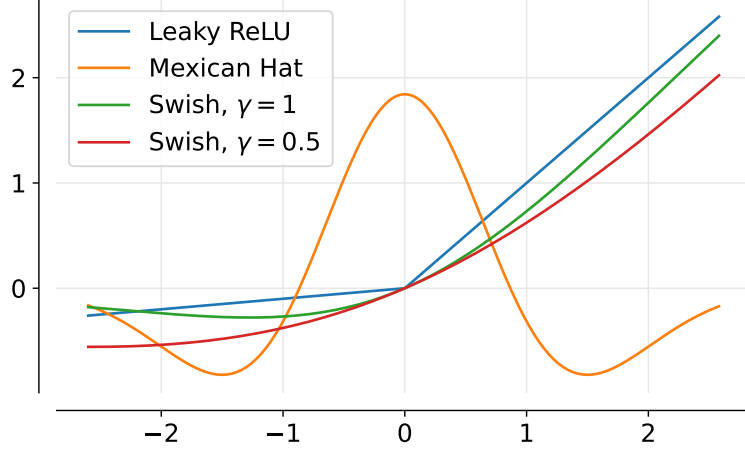


Figure S1 Dendritic activation functions explored in our study.

We explore four types of dendritic nonlinear activation in our study, as shown in Figure S1 and Equation (S1). **Leaky ReLU** is a common choice of activation function in artificial neural networks. It imposes a small gradient in the negative part, allowing dendrites to have suppressive effects on the soma. **Mexican hat** is a bell-shaped function that resembles the receptive field of a simple cell in the visual cortex. It is defined as the second derivative of a Gaussian function, whose parameters are set according to Equation (S1). Here, we adopt the Mexican hat function to mimic the non-monotonic influence of dendrites on the soma induced by calcium-mediated dendritic action potentials (dCaAPs) [1]. Notice that the value of the Mexican hat function can be negative, enabling us to model dendritic inhibitory effects on the soma. That’s why we use the Mexican hat function instead of the Gaussian function in our experiments. **Swish** is an activation function parameterized by a learnable scalar γ [2]. If $\gamma = 0$, Swish degrades to a linear function $f(x) = x/2$; if $\gamma \rightarrow +\infty$, Swish approaches the ReLU function. In our experiments, γ is initialized by sampling from a log-normal distribution with mean 0 and standard deviation 1 (i.e. $\ln \gamma \sim \mathcal{N}(0, 1)$). Besides, we consider a variant of Swish, named **USwish**, whose slope γ is fixed to its initial value.

$$\begin{aligned}
 \text{Leaky ReLU} : f^{\text{LReLU}}(x) &= \begin{cases} x & x \geq 0 \\ 0.01x & x < 0 \end{cases} \\
 \text{Mexican hat} : f^{\text{MH}}(x) &= \frac{d^2}{dx^2} 3\phi(x; \mu = 0, \sigma^2 = 0.75) \\
 &= \frac{0.75 - x^2}{0.75^2 \sqrt{2\pi} \times 0.75} \exp\left[-\frac{(x-0)^2}{2 \times 0.75}\right] \\
 \text{Swish, USwish} : f^{\text{Swish}}(x; \gamma) &= x\sigma(\gamma x) = \frac{x}{1 + \exp(-\gamma x)}
 \end{aligned} \tag{S1}$$

The choice of dendritic branch activation function is crucial for the performance of DendSNNs. We find that the Mexican hat function works extraordinarily well on shallow fully connected networks, such as the one we adopted in FashionMNIST-based experiments. Moreover, Figure 6b in the main text demonstrates that Mexican hat significantly enhances DendSNNs’ robustness against adversarial attacks. However, if convolutional architectures are used (like SEW ResNets [3] and the toy network with two spiking neuron layers used in the N-MNIST experiment), the optimization of Mexican hat DendSNNs often fails. As demonstrated in Figure S2, in the first neuron layer of a Mexican hat DendSNN, neurons have much higher firing rates compared to neurons in a point SNN. If T is set to 8, these neurons will always fire (firing rate is nearly 1), which is not desirable for hierarchical signal propagation and cannot convey discriminative information. To be worse, Mexican hat DendSNNs in deeper layers can hardly fire under $T = 8$ condition soon after the training process starts (see Table S1 and the lower right subplot of Figure S2). This troublesome phenomenon hinders the forward pass of information and the backward pass of gradients. Consequently, model parameters cannot be updated. The other three activation types, unbounded at their positive parts, mitigate this issue and are thus more suitable for deeper convolutional SNNs. Figure S2 indicates that neurons in the first layer of a leaky ReLU DendSNN

have similar firing rates to point neurons. What’s more, neurons in the second layer of a leaky ReLU DendSNN under $T = 8$ condition possess higher firing rates than point neurons and Mexican hat DendSNNs, while still maintaining a moderate level. This might be one of the reasons why leaky ReLU activation leads to better training accuracies on N-MNIST if $T = 8$ (Table S1). We also find that Swish and USwish DendSNNs have similar firing rate patterns to leaky ReLU DendSNNs. Although they might sometimes fail at PFA conditions (Table S3) due to the small value of \mathbf{K} generated by the attention mechanism, their performances on “none” and “ \mathbf{K} learnable” conditions are comparable to that of leaky ReLU DendSNNs. Accordingly, we **report the results of Mexican hat activation for our experiments on the FashionMNIST dataset in the main text; in other experiments where complex model structures are used, we report the results adopting the activation function that obtains the best performance among the three unbounded activation types.**

Table S1 The training accuracies on the N-MNIST datasets after training for 50 epochs, as well as the overall firing rate of the spiking neurons in the second neuron layer (in front of the fully connected classification head).

Neuron Type		T=4		T=8	
Dend. Activation	#Branches	Acc. (%)	Firing Rate	Acc. (%)	Firing Rate
Mexican hat	B=1	99.46	0.198	<u>11.24</u>	<u>0.000</u>
	B=2	98.62	0.141	<u>11.24</u>	<u>0.000</u>
leaky ReLU	B=1	98.35	0.149	98.26	0.169
	B=2	98.74	0.188	98.61	0.176
point SN		<u>90.05</u>	<u>0.012</u>	97.04	0.105

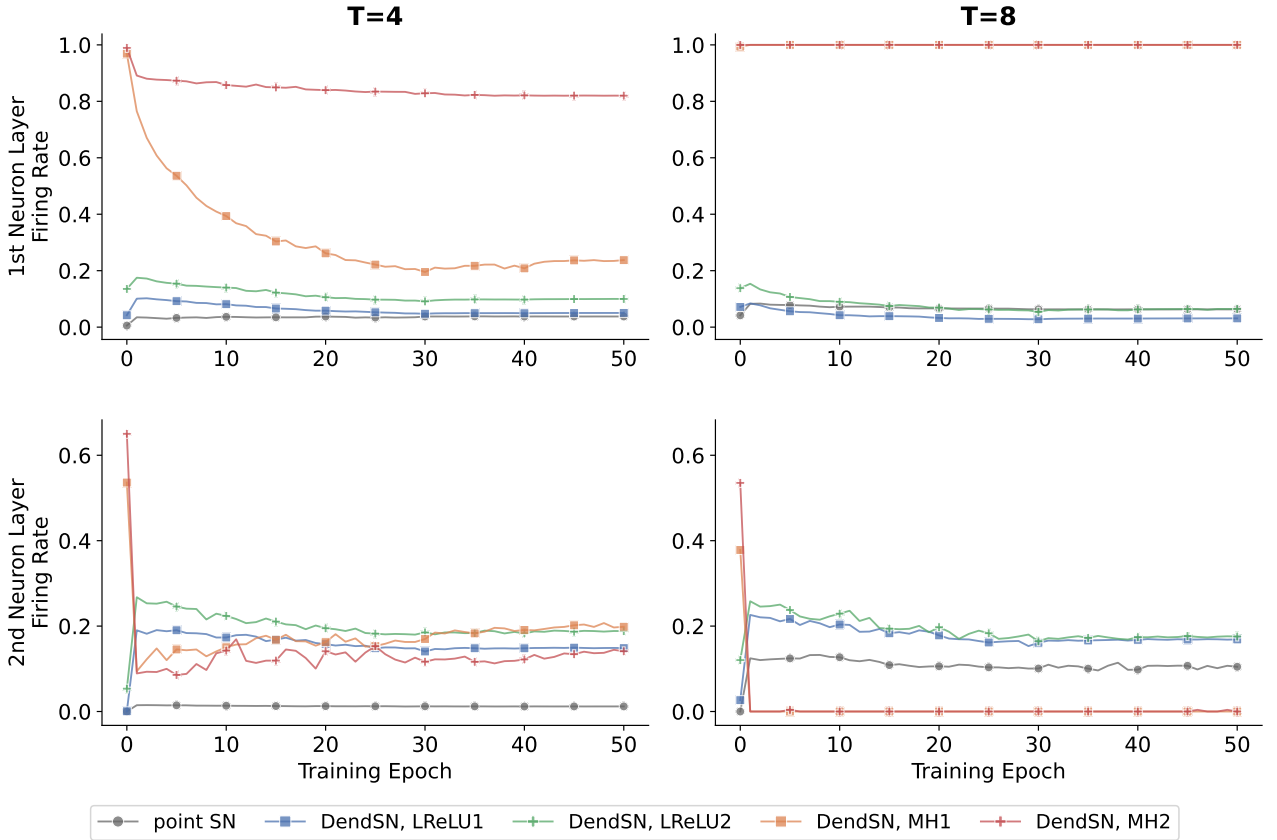


Figure S2 Spiking neuron layers’ firing rates after the networks are trained on N-MNIST for a given number of epochs. The convolutional network architecture is illustrated in 4 of the main text. Firing rates are calculated using the validation set as network input. Notice that when $T = 8$, DendSNNs with Mexican hat nonlinearity located in the 2nd layer do not fire at all (firing rate is zero; see the lower right subplot), while those located in the 1st layer always fire (firing rate is 1; see the upper right subplot).

S2 PyTorch implementations of a DendSN layer

Here, we provide two PyTorch implementations of a DendSN layer. Besides PyTorch, we import SpikingJelly [4], an open-source deep SNN programming framework based on PyTorch, for its spiking functions with surrogate gradients. Notice that these code snippets are simplified for better readability. For our full implementation in an object-oriented style, please refer to the source code at <https://github.com/AllenYolk/dbg-experiments>, which will be publicly available once the paper is published.

```
1 import torch
2 from spikingjelly.activation_based import surrogate
3 from typing import Callable
4
5
6 def dendsn_forward(
7     x_seq: torch.Tensor, # input; shape = [T, N, C, *], * for spatial dims
8     B: int, # number of branches
9     alpha: torch.Tensor, # dendritic time constant; shape = [1]
10    k: torch.Tensor, # broadcastable to [T, N, C // B, B, L]
11    f_dact: Callable, # element-wise dendritic activation function
12    beta: torch.Tensor, # somatic time constant; shape = [1]
13    v_th: torch.Tensor = torch.Tensor([1.]), # firing threshold
14    v_reset: torch.Tensor = torch.Tensor([0.]), # reset potential
15    sg: Callable = surrogate.ATan(), # spiking function with sg
16 ):
17     expected_out_shape = list(x_seq.shape)
18     x_seq = x_seq.unsqueeze(-1).flatten(3) # shape = [T, N, C, L]
19     T, N, C, L, dtype, device = *x_seq.shape, x_seq.dtype, x_seq.device
20     expected_out_shape[2] = C // B # should be [T, N, C//B, *]
21     x_seq = x_seq.view(T, N, C // B, B, L) # fold along the channel dim
22
23     # states: dendritic potential and somatic potential
24     v_d = torch.zeros_like(x_seq[0]) #shape = [N, C // B, B, L]
25     v_s = torch.zeros([N, C // B, L], dtype=dtype, device=device)
26
27     spike_seq = []
28     for t in range(T):
29         # dendritic local dynamics
30         v_d = alpha*v_d + x_seq[t]
31         # dendrite-to-soma forwarding
32         y = k * f_dact(v_d) # shape = [N, C // B, B, L]
33         y = y.sum(3) # shape = [N, C // B, L]
34         # LIF soma
35         v_s = beta*v_s + (1-beta) * y # assume v_rest = 0
36         spike = sg(v_s - v_th)
37         spike_seq.append(spike)
38         v_s = (1.-spike) * v_s + spike*v_reset
39
40     return torch.stack(spike_seq).view(expected_out_shape)
```

Listing S1 PyTorch implementation of a DendSN layer.

```

1 import torch
2 from spikingjelly.activation_based import surrogate
3 from typing import Callable
4
5 alpha_for_matrix, T_for_matrix, alpha_matrix = None, None, None
6
7
8 def dendsn_forward_accelerated(
9     x_seq: torch.Tensor, # input; shape = [T, N, C, *], * for spatial dims
10    B: int, # number of branches
11    alpha: torch.Tensor, # dendritic time constant; shape = [1]
12    k: torch.Tensor, # broadcastable to [T, N, C // B, B, L]
13    f_dact: Callable, # element-wise dendritic activation function
14    beta: torch.Tensor, # somatic time constant; shape = [1]
15    v_th: torch.Tensor = torch.Tensor([1.]), # firing threshold
16    v_reset: torch.Tensor = torch.Tensor([0.]), # reset potential
17    sg: Callable = surrogate.ATan(), # spiking function with sg
18 ):
19     expected_out_shape = list(x_seq.shape)
20     x_seq = x_seq.unsqueeze(-1).flatten(3) # shape = [T, N, C, L]
21     T, N, C, L, dtype, device = *x_seq.shape, x_seq.dtype, x_seq.device
22     expected_out_shape[2] = C // B # should be [T, N, C//B, *]
23     x_seq = x_seq.view(T, N, C // B, B, L) # fold along the channel dim
24
25     # set the alpha matrix
26     global alpha_matrix, alpha_for_matrix, T_for_matrix
27     if alpha_for_matrix != alpha or T_for_matrix != T:
28         alpha_for_matrix, T_for_matrix = alpha, T
29         alpha_matrix = torch.empty([T, T], dtype=dtype, device=device)
30         for i in range(T):
31             for j in range(0, i + 1):
32                 alpha_matrix[i, j] = alpha**(i - j)
33
34     # dendritic dynamics and dendrite-to-soma forwarding
35     v_d_seq = alpha_matrix.view(T, T, 1, 1, 1, 1) * x_seq
36     v_d_seq = v_d_seq.sum(1) # shape = [T, N, C // B, B, L]
37     y_seq = k * f_dact(v_d_seq) # shape = [T, N, C // B, B, L]
38     y_seq = y_seq.sum(3) # shape = [T, N, C // B, L]
39
40     # LIF soma
41     v_s = torch.zeros([N, C // B, L], dtype=dtype, device=device)
42     spike_seq = []
43     for t in range(T):
44         v_s = beta*v_s + (1-beta) * y_seq[t] # assume v_rest = 0
45         spike = sg(v_s - v_th)
46         spike_seq.append(spike)
47         v_s = (1.-spike) * v_s + spike*v_reset
48
49     return torch.stack(spike_seq).view(expected_out_shape)

```

Listing S2 PyTorch implementation of a DendSN layer with temporally parallel dendritic state update.

S3 Dense weights v.s. sparse weights in dendritic neural networks

Take the following block in a point SNN as an example:

$$\text{FC}(m \rightarrow n) \Rightarrow \text{PointNeuron}(n) \Rightarrow \text{FC}(n \rightarrow p) \Rightarrow \text{PointNeuron}(p) \quad (\text{S2})$$

Assume the input has shape $[m]$. The output of this block should have shape $[p]$. The computational complexity of this block is

$$C_{\text{point}} = O(mn + n + np + p) = O(mn + np) \quad (\text{S3})$$

Previous works on dendritic deep learning add a sparsity constraint on the weight layer preceding the neuron layer [5, 6]. To convert point neurons to dendritic neurons, these works replace the original fully connected layers with larger fully connected layers $\text{FC}(m \rightarrow nb), \text{FC}(n \rightarrow pb)$, where b is the number of branches in a dendritic neuron. The weight matrix of the new fully connected layer has sparsity $\rho = \frac{1}{b}$, thus having the same number of learnable parameters as the original one. The dendritic neuron layer then convert the nb features to n features, yielding the same output shape as the original block.

$$\text{SparseFC}(m \rightarrow nb, \rho = \frac{1}{b}) \Rightarrow \text{DendSN}(n, b) \Rightarrow \text{SparseFC}(n \rightarrow pb, \rho = \frac{1}{b}) \Rightarrow \text{DendSN}(p, b) \quad (\text{S4})$$

Here, $\text{DendSN}(n, b)$ means a dendritic neuron layer containing n neurons, each with b branches. Assuming the input has shape $[m]$, the computational complexity of this block is

$$C_{\text{dend,sparse}} = O(mnb + nb + npb + pb) = O(mnb + npb) \quad (\text{S5})$$

In our work, we use dense weight matrices while scaling the number of features by b or $\frac{1}{b}$. The block in Equation (S2) can be converted to

$$\text{FC}(m \rightarrow n) \Rightarrow \text{DendSN}(\frac{n}{b}, b) \Rightarrow \text{FC}(\frac{n}{b} \rightarrow pb) \Rightarrow \text{DendSN}(p, b) \quad (\text{S6})$$

Assuming the input has shape $[m]$, the computational complexity of this block is

$$C_{\text{dend,dense}} = O(mn + \frac{n}{b}b + \frac{n}{b}pb + pb) = O(mn + np) \quad (\text{S7})$$

Thus, the computational complexity of a block in a dendritic neural network with dense weights is the same as that of the corresponding block in a point SNN, much lower than that of the corresponding block in a dendritic neural network with sparse weights.

S4 Supervised learning results

Figure 3 presents only a part of the supervised learning results. Here, we provide the complete results of the supervised learning experiments on FashionMNIST and N-MNIST datasets in Table S2 and S3.

Table S2 FashionMNIST supervised learning performance. We report test accuracies (%) here. “learnable” means that $\mathbf{K}_{T \times B}$ is fully learnable; “PFA” stands for parameter-free attention; “MA” stands for multi-dimensional attention. Underline means the model cannot be trained.

Neuron Type		K rule			
Dendritic Activation	#Branches	none	learnable	PFA	MA
Mexican hat	1	90.37	90.31	89.89	<u>10.00</u>
	2	90.04	89.95	90.60	<u>10.00</u>
	5	90.19	89.88	90.23	89.94
leaky ReLU	1	90.02	90.04	89.76	<u>10.00</u>
	2	90.36	90.45	89.64	87.68
	5	90.36	90.53	90.15	89.07
Swish	1	89.67	89.71	89.25	48.41
	2	89.63	89.96	89.58	88.35
	5	90.15	90.03	89.99	88.35
USwish	1	89.98	89.63	89.09	<u>10.00</u>
	2	90.18	89.72	89.57	88.20
	5	89.90	90.09	89.49	87.94
point SN		88.97	-	-	-

Table S3 N-MNIST supervised learning performance. We report test accuracies (%) here. “learnable” means that $\mathbf{K}_{T \times B}$ is fully learnable; “PFA” stands for parameter-free attention. Underline means the model cannot be trained.

Neuron Type		T=4			T=8		
Dendritic Activation	#Branches	none	learnable	PFA	none	learnable	PFA
Mexican hat	1	98.73	98.92	98.65	98.87	98.76	98.62
	2	93.81	<u>11.35</u>	98.69	<u>11.35</u>	<u>11.35</u>	<u>11.35</u>
leaky ReLU	1	98.13	97.92	97.42	98.10	97.63	98.06
	2	98.35	98.39	97.36	98.35	98.41	98.14
Swish	1	95.14	96.60	<u>11.35</u>	97.26	96.98	<u>11.35</u>
	2	96.57	96.43	<u>11.35</u>	98.04	98.07	97.42
USwish	1	96.96	97.31	<u>11.35</u>	97.71	97.59	96.37
	2	97.76	98.05	96.79	98.03	98.06	97.3
point SN		96.02	-	-	97.27	-	-

S5 Pseudocodes of dendritic branch gating

Algorithm S1 describes the forward pass of a DendSNN with DBG. Besides the input tensor \mathbf{X} , a task index q is also fed into the model as a modulation signal. A mapping from task index to branch strength matrices, DBG, is required by the algorithm, too. For possible implementations of *DBG* mapping, please refer to [Methods](#) in the main text. Algorithm S2 and Algorithm S3 show how to use DBG in continual (task incremental) learning and multitask learning settings. All we need to do is to replace the forward pass in these pipelines with DBGForward (Algorithm S1), and of course provide the model with task index q . Following this strategy, we may extend DBG to other task-context-aware learning scenarios.

Notice that in the algorithms described here, DBG mapping and branch strength modulation are calculated each time before the forward pass. However, as the modulated strength values depend only on q , not on input data \mathbf{X} , we may calculate the mapping and set the strengths once and then conduct the forward pass on the specific task multiple times. We use this optimization during both the training and inference phases of continual learning in order to save time.

Algorithm S1 DBGForward($\mathbf{X}, q, f_{\text{DendSNN}}, \text{DBG}$)

Require: \mathbf{X} , input tensor to the DendSNN

Require: q , index of the current task

Require: f_{DendSNN} , the DendSNN model

Require: DBG, the DBG function mapping from task index to branch strength matrices

Ensure: \mathbf{Y} , output tensor of the DendSNN

```

1: for each DendSN layer  $l$  in  $f_{\text{DendSNN}}$  do    // Modulate  $\mathbf{K}$  using DBG.
2:    $\{\mathbf{K}^{(n)}\}_{n=0}^{N_l-1} \leftarrow \text{DBG}(q)$ 
3:   Set the  $N_l$  branch strength matrices of the  $N_l$  DendSNs in  $l$  to  $\{\mathbf{K}^{(n)}\}_{n=0}^{N_l-1}$ 
4: end for
5:  $\mathbf{Y} \leftarrow f_{\text{DendSNN}}(\mathbf{X})$     // Forward pass, with branch strengths modulated.
6: return  $\mathbf{Y}$ 

```

Algorithm S2 Task incremental Learning with dendritic branch gating (DBG)

Require: $\{D_q^{\text{train}}\}_{q=0}^{Q-1}$, training sets of Q tasks

Require: $\{D_q^{\text{test}}\}_{q=0}^{Q-1}$, test sets of Q tasks

Require: \mathcal{L} , the loss function

Require: f_{DendSNN} , the DendSNN model to be trained and evaluated

Require: DBG, the DBG function mapping from task index to branch strength masks

```

1: for  $q \leftarrow 0$  to  $Q - 1$  do    // Learn the  $Q$  tasks sequentially.
2:   for  $(\mathbf{X}, \mathbf{Y}) \in D_q^{\text{train}}$  do
3:     $\hat{\mathbf{Y}} \leftarrow \text{DBGForward}(\mathbf{X}, q, f_{\text{DendSNN}}, \text{DBG})$ 
4:    Update the parameters in  $f_{\text{DendSNN}}$  using BP and gradient descent according to  $\mathcal{L}(\hat{\mathbf{Y}}, \mathbf{Y})$ 
5:   end for
6: end for
7: for  $q \leftarrow 0$  to  $Q - 1$  do    // Evaluate the model on the test sets.
8:   for  $(\mathbf{X}, \mathbf{Y}) \in D_q^{\text{test}}$  do
9:     $\hat{\mathbf{Y}} \leftarrow \text{DBGForward}(\mathbf{X}, q, f_{\text{DendSNN}}, \text{DBG})$ 
10:   Compute the test loss  $\mathcal{L}(\hat{\mathbf{Y}}, \mathbf{Y})$  and other evaluating metrics
11:   end for
12: end for

```

Algorithm S3 Multitask Supervised Learning with dendritic branch gating (DBG)

Require: $\{D_q^{\text{train}}\}_{q=0}^{Q-1}$, training sets of Q tasks
Require: $\{D_q^{\text{test}}\}_{q=0}^{Q-1}$, test sets of Q tasks
Require: \mathcal{L} , the loss function
Require: f_{DendSNN} , the DendSNN model to be trained and evaluated
Require: DBG, the DBG function mapping from task index to branch strength masks
Require: I_{max} , the maximum number of training iterations

- 1: *// Sample training data randomly from the Q tasks, for I_{max} iterations.*
- 2: **for** $i \leftarrow 0$ to $I_{\text{max}} - 1$ **do**
- 3: Sample a task index q from $\{0, 1, \dots, Q - 1\}$
- 4: Sample a (batch of) training sample(s) (\mathbf{X}, \mathbf{Y}) from D_q^{train}
- 5: $\hat{\mathbf{Y}} \leftarrow \text{DBGForward}(\mathbf{X}, q, f_{\text{DendSNN}}, \text{DBG})$
- 6: Update the parameters in f_{DendSNN} using BP and gradient descent according to $\mathcal{L}(\hat{\mathbf{Y}}, \mathbf{Y})$
- 7: **end for**
- 8: **for** $q \leftarrow 0$ to $Q - 1$ **do** *// Evaluate the model on all the test sets.*
- 9: **for** $(\mathbf{X}, \mathbf{Y}) \in D_q^{\text{test}}$ **do**
- 10: $\hat{\mathbf{Y}} \leftarrow \text{DBGForward}(\mathbf{X}, q, f_{\text{DendSNN}}, \text{DBG})$
- 11: Compute the test loss $\mathcal{L}(\hat{\mathbf{Y}}, \mathbf{Y})$ and other evaluating metrics
- 12: **end for**
- 13: **end for**

S6 Permuted MNIST continual learning results

Figure 4f presents only a part of the Permuted MNIST results. Here, we provide the complete results of this experiment in Table S4. Notice that we also show the results of applying XdG to DendSNNs in this table.

Table S4 Permuted MNIST task incremental learning performance. Average test accuracies (%) over all the 50 tasks are reported. $i\%$ stands for sparsity.

Neuron Type		Strategy								
Dend. Activation	#Branches	none	DBG-1hot	DBG-embedding	DBG-random			XdG		
					1%	2%	5%	1%	2%	5%
Mexican hat	1	24.44	-	29.25	72.60	80.70	75.74	72.49	79.33	77.39
	5	19.36	35.04	27.91	81.12	82.16	81.48	34.18	60.69	60.38
	10	17.96	54.26	28.88	78.27	81.46	77.15	11.29	10.74	10.41
	25	11.35	83.47	31.98	76.97	80.39	74.67	11.21	10.97	10.36
	50	11.35	94.05	36.83	73.53	76.00	72.48	11.19	10.75	10.39
point SN		34.65	-	-	-	-	-	77.13	84.25	74.25

S7 Multitask learning

Here, we discuss the possibility of using DendSNNs and DBG in multitask learning settings. We want to show that the application of DBG is not limited to continual learning.

In a multitask learning setting, a model aims to learn Q tasks $\{D_q\}_{q=0}^{Q-1}$ simultaneously, in a supervised manner. Besides the feedforward input, the model is also provided with the index q of the task it is currently working on. We can easily extend our DBG algorithm to multitask learning setups, as Algorithm S3 describes.

Here, we focus on multi-output learning [7], a special case of multitask learning, where different tasks share the same input data but have different target values. To empower neural networks with multitask learning capabilities, we set multiple parallel output heads on top of a shared feature extractor. Each head is trained to solve one specific task, while the feature extractor has the potential to learn shared representations underlying all tasks. In a training iteration, a task index q is randomly sampled from $\{0, 1, \dots, Q-1\}$. The model is then optimized with the loss of the q -th task, which is computed by the output of the corresponding head. We find that randomly sampling tasks in each iteration yields better performance than optimizing the model using the overall loss.

Next, we present two multitask learning experiments to demonstrate the effectiveness of our models and algorithm in multitask learning scenarios.

In the Multi-(Fashion+MNIST) [8] experiment, each input sample is a grey-scale image of size 36×36 . An MNIST digit is placed at the top-left corner of an image, while a FashionMNIST icon is located at the bottom-right, partially overlapped with the former one (Figure S3a). The goal of to classify these two items simultaneously. We adopt a convolutional network with two Conv2d layers and two parallel classification heads. Other settings resemble those of supervised learning tasks, and the hyperparameters are demonstrated in Table S8. As shown in Figure S3b, nearly all the DendSNNs outperform the point SNN baseline. DBG_{random} with sparsity $\rho = 0.4$ achieves the best performance on both MNIST and FashionMNIST subtasks. Furthermore, we experiment again, using a fully connected network architecture. As summarized in Table S5, under most conditions, DendSNNs’ performances are inferior to point SNN’s. Only three out of the twenty conditions have better performances on both MNIST and FashionMNIST subtasks.

Table S5 Multi-(Fashion+MNIST) multitask learning performance. Accuracies (%) on the two subtasks (FashionMNIST and MNIST) are reported. “FC” is a two-layer fully connected SNN, while “CNN” uses two convolutional blocks as the feature extractor and one fully connected layer as the classification head. Numbers under “DBG-random” stand for sparsity.

Network Type	Neuron Type		FashionMNIST Accuracy (%)						
	Dend. Activation	#Branches	none	DBG-1hot	DBG-embedding	DBG-random			
						20%	40%	60%	80%
FC	leaky ReLU	1	82.58	-	83.38	82.38	82.56	83.08	82.62
		2	82.33	83.87	83.28	82.40	83.27	83.03	81.52
		5	80.71	82.38	82.85	82.34	82.24	81.85	81.85
	point SN		82.77	-	-	-	-	-	-
CNN	leaky ReLU	1	87.40	-	88.08	87.17	88.06	87.31	87.12
		2	87.09	87.36	87.39	87.72	88.64	87.42	86.76
		5	86.92	87.56	87.16	87.91	87.72	87.65	86.54
	point SN		86.80	-	-	-	-	-	-
Network Type	Neuron Type		MNIST Accuracy (%)						
	Dend. Activation	#Branches	none	DBG-1hot	DBG-embedding	DBG-random			
						20%	40%	60%	80%
FC	leaky ReLU	1	87.10	-	87.81	84.75	86.83	87.63	87.37
		2	86.77	87.96	88.04	85.53	87.60	87.96	85.30
		5	84.66	86.39	86.61	85.78	85.60	85.12	85.82
	point SN		87.91	-	-	-	-	-	-
CNN	leaky ReLU	1	96.14	-	96.69	95.22	96.77	96.76	96.61
		2	96.29	96.96	97.04	96.23	97.08	96.92	96.73
		5	95.86	96.86	96.71	96.57	96.81	96.95	96.61
	point SN		95.74	-	-	-	-	-	-

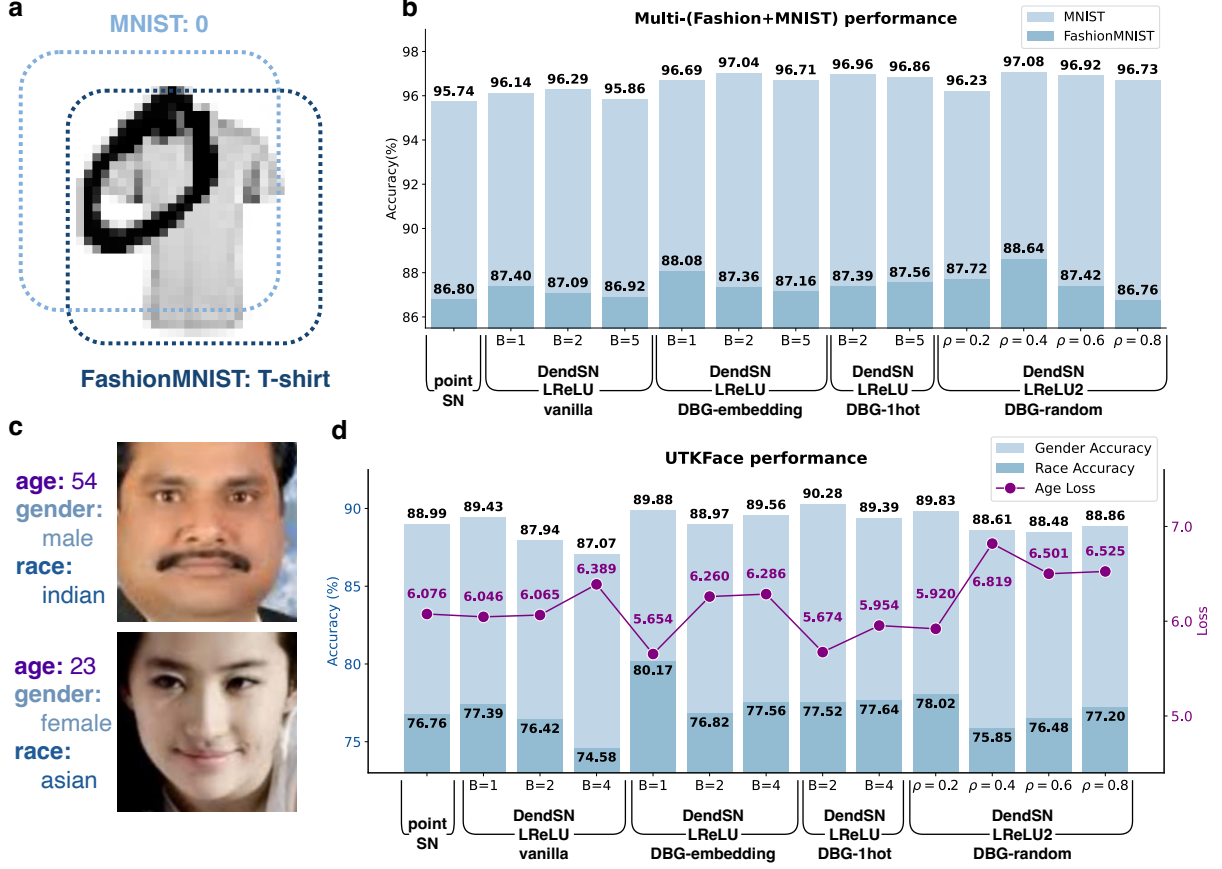


Figure S3 DendSNNs' multitask learning performances. **a**) Multi-(Fashion+MNIST) setup. **b**) The performance of different models on Multi-(Fashion+MNIST). All DendSNNs outperform the point SNN baseline. **c**) UTKFace setup. **d**) The performance of different models on UTKFace. 6 out of the 12 DendSNNs outperform the point SNN baseline on all three metrics.

In the UTKFace [9] experiment, the inputs are RGB images of aligned and cropped human faces rescaling to size 128×128 . The training samples are labeled with gender, race, and age, so we formulate these tasks as binary classification, 5-way classification, and regression problems, respectively (Figure S3c). The network we use has a SEW ResNet18 backbone and three parallel output heads. We use cross-entropy losses for classification subtasks, and mean absolute error (MAE) loss for age regression. The training follows the procedure of the FashionMNIST supervised training experiment, and the hyperparameters are listed in Table S8. Figure S3d suggest that 6 out of the 12 DendSNNs get better results than point SNN on all three metrics, with $\text{DBG}_{\text{embedding}} (B = 1)$ being the best model. A detailed view of the results is demonstrated in Table S6.

Taken together, DendSNNs with $\text{DBG}_{\text{embedding}}$ and $\text{DBG}_{\text{random}}$ (ρ should be small) can obtain marginally better results on multitask learning scenarios. Compared to continual learning settings, this improvement seems to be less obvious and consistent; under certain circumstances, the introduction of dendritic computing and DBG may lead to performance degradation. That's because the "shared-extractor, task-specific head" architecture is actually powerful enough to handle multitask learning problems, making the space for improvement by DBG limited. Also, multitask learning emphasizes shared representations across different tasks. DBG, aiming to reduce the interference between tasks, may not be the best choice in this case.

Table S6 UTKFace multitask learning performance. Accuracies (%) of gender/race classification and the mean absolute error of age regression are reported. Numbers under “DBG-random” mean sparsity.

Neuron Type		Gender Accuracy (%)						
Dend. Activation	#Branches	none	DBG-1hot	DBG-embedding	DBG-random			
					20%	40%	60%	80%
leaky ReLU	1	89.43	-	89.88	88.04	88.74	88.95	89.77
	2	87.94	90.28	88.97	89.83	88.61	88.48	88.86
	4	87.07	89.39	89.56	87.37	88.65	89.01	88.82
point SN		88.99	-	-	-	-	-	-
Neuron Type		Race Accuracy (%)						
Dend. Activation	#Branches	none	DBG-1hot	DBG-embedding	DBG-random			
					20%	40%	60%	80%
leaky ReLU	1	77.39	-	80.17	74.18	76.95	75.57	75.62
	2	76.42	77.52	76.82	78.02	75.85	76.48	77.20
	4	74.58	77.64	77.56	75.89	75.28	74.56	76.42
point SN		76.76	-	-	-	-	-	-
Neuron Type		Age MAE						
Dend. Activation	#Branches	none	DBG-1hot	DBG-embedding	DBG-random			
					20%	40%	60%	80%
leaky ReLU	1	6.046	-	5.654	6.531	6.553	6.827	6.619
	2	6.065	5.674	6.260	5.920	6.819	6.501	6.525
	4	6.389	5.954	6.286	6.760	6.840	6.441	6.516
point SN		6.076	-	-	-	-	-	-

S8 DVS Gesture-C dataset

To investigate DendSNNs’ robustness against various types of noises added directly to event data (rather than static images), we construct a new corrupted dataset based on DVS Gesture. A total of 6 types of corruptions are applied to the spike train data in the original DVS Gesture test set, each with 5 levels of severity. These corruptive transforms are implemented using the Tonic API [10]. Table S7 shows the detailed parameters for generating the DVS Gesture-C dataset, and a visualization of the corrupted samples can be found in Figure 5g in the main text.

Table S7 Parameters for generating DVS Gesture-C dataset.

Corruption Type	Description	Severity				
		1	2	3	4	5
drop pixel	drop pixels completely that fire higher than the given frequency f	30	25	20	15	10
drop event	randomly drops events with probability p	0.16	0.32	0.48	0.64	0.80
refractory period	set a refractory period t (unit: ms) for each pixel, during which events will be discarded	7.5	15.0	22.5	30.0	37.5
time jitter	changes timestamp for each event by adding a standard Gaussian noise with sd σ (unit: s)	0.5	1.0	1.5	2.0	2.5
spatial jitter	changes x/y coordinate for each event by adding a multivariate Gaussian noise with var σ^2	0.3	0.6	0.9	1.2	1.5
uniform noise	adds a fixed number of n noise events that are uniformly distributed	40k	80k	120k	160k	200k

S9 Hyperparameter settings for the experiments

Here, we provide the hyperparameter settings for the experiments mentioned in the main text (except for the simulation efficiency experiment, which has been completely illustrated in [Methods](#)), as well as the multitask learning experiments described in Supplementary Information [S7](#). For the model architectures adopted in these experiments and more details about experiment settings, please refer to the source code at <https://github.com/AllenYolk/dbg-experiments>, which will be publicly available once the paper is published.

Table S8 Hyperparameter settings. **T** means number of simulation time steps, while **lr** means learning rate. Learning rate schedulers: "cosine" has a period of 80 and a minimal learning rating of 5×10^{-4} ; "multistep-1" scheduler scales the learning rate at epoch ($\#epochs-20$) with factor 0.25; "multistep-2" scales the learning rate at epoch ($\#epochs-20$) and ($\#epochs-10$) with factor 0.25; "multistep-3" scales the learning rate at epoch ($\#epochs-50$) and ($\#epochs-20$) with factor 0.25; "multistep-4" scales the learning rate at epoch ($\#epochs-30$) and ($\#epochs-15$) with factor 0.25; "multistep-5" scales the learning rate at epoch ($\#epochs-100$) and ($\#epochs-40$) with factor 0.25.

	Experiment	T	#epochs	batch size	initial lr	lr scheduler	others	
	single neuron approximation	L5PC	2048	200	32	10^{-3}	cosine	-
supervised learning	FashionMNIST	4	100	128	10^{-4}	multistep-1	-	
	N-MNIST	4, 8	50	64	10^{-3}	multistep-2	-	
continual learning	Permuted MNIST	4	8	128	10^{-4}	none	#tasks=50	
	Split CIFAR-100	4	250	32	10^{-3}	multistep-3	#tasks=10	
	Split TinyImageNet	4	150	32	10^{-3}	multistep-3	#tasks=20	
multitask learning	Multi-(Fashion+MNIST)	4	75	32	10^{-3}	multistep-4	#task=2	
	UTKFace	4	150	16	10^{-3}	multistep-3	#task=3	
noise robustness	FashionMNIST-noise	4	100	128	10^{-4}	multistep-1	-	
	CIFAR-10-C	4	300	32	10^{-3}	multistep-5	-	
	TinyImageNet-C	4	300	128	10^{-3}	multistep-5	-	
	DVS Gesture-C	4	150	16	10^{-4}	multistep-3	-	
robustness against adversarial attack	FashionMNIST-adv	4	100	128	10^{-4}	multistep-1	-	
few-shot learning	miniImageNet-episodic	4	300	128	10^{-3}	multistep-5	-	
	miniImageNet-classical	4	300	128	2×10^{-4}	multistep-5	#query-per-class=15 #episode-per-epoch=500	

Table S9 Neuronal parameters. The same neuronal parameters are used for all experiments.

Neuronal Parameter	α dendritic potential decay factor	β somatic potential decay factor	V_{rest}^d dendritic resting potential	V_{rest} somatic resting potential	V_{reset} somatic reset potential	V_{th} somatic firing threshold
Value	0.5	0.5	0.0	0.0	0.0	1.0

S10 Limitations and future directions

We summarize the limitations of our work from three aspects, and propose future research directions according to them.

Scalability

While significant progress has been made in incorporating dendritic computing into deep spiking neural networks, scaling up to larger models and datasets remains a challenge. We have extended dendritic spiking neural networks to depths comparable to prevalent point SNNs through parallelization of dendritic state update across time steps and introducing Triton kernels, making the utilization of deep SNN architectures like SEW ResNet18 [3] and Spike-driven Transformer [11] possible by dendritic computation. However, there remains a noticeable gap between DendSNNs and state-of-the-art deep networks (either SNNs or ANNs), in terms of both the model size and their performance on large-scale tasks. Although theoretically, DendSNNs can be extended to architectures of arbitrary depth, we have not yet explored the feasibility of training extremely deep DendSNNs. Furthermore, even though DendSNNs can exhibit promising performance on tasks with intermediate complexity like TinyImageNet and UTKFace, they may struggle to match the absolute accuracy achieved by point SNNs on extremely large datasets such as ImageNet [12]. Our future research efforts will aim to power up DendSNNs for large-scale tasks by refining network structures and training methodologies.

Task diversity

Our experiments primarily focus on classification tasks involving static image or event stream data, limiting the scope of tasks explored in this work. While we have investigated various scenarios including supervised learning, continual learning, multitask learning, robustness against noise and adversarial attacks, as well as few-shot learning, there is potential to extend the application of DendSNNs to a broader range of tasks and modalities. Spiking neural networks have demonstrated effectiveness in tasks beyond visual classification, such as object detection and tracking in high-speed scenes [13]. Additionally, the inherent capabilities of SNNs with dendritic structures in processing input with rich time scales suggest their potential applications in tasks requiring fine-grained temporal processing, as stated by Zheng et al. [6]. Our future research will explore the application of DendSNNs in diverse real-world scenarios, expanding beyond the confines of image classification.

Biological plausibility

While DendSN offers enhanced biological plausibility compared to point spiking neurons due to its dendritic morphological and nonlinear dynamics, there are still limitations to its biological fidelity. As Figure 2f suggests, even with fully learnable dendritic branch strengths, DendSN may not fully capture the complex activity patterns observed in biological neurons, particularly when the somatic potential is near the firing threshold. This discrepancy arises from the necessary simplifications made to the neuron model so as to ensure low computational overhead. Future research may explore alternative approaches to incorporate dendritic nonlinearity while maintaining computational efficiency, such as the design of new specialized dendritic activation functions.

Additionally, the reliance on gradient-based backpropagation for learning in DendSNNs raises concerns regarding biological plausibility. In the current work, DendSNNs are optimized through STBP [14], an intuitive extension of backpropagation to both temporal and spatial dimensions of SNNs. By propagating signed global error signals downstream along another backward pathway, whose weights are constrained to be strictly symmetric to the forward pathway, this gradient-based credit assignment rule leads to ideal optimization results in supervised learning scenarios. However, neuroscientists have underscored that there are fatal difficulties in implementing BP-like learning in biological neural circuits, since the requirements of weight symmetry and signed error signals can hardly be satisfied in the brain [15]. This opinion poses a challenge to the biological feasibility of DendSNNs' training. Our future investigations will delve into exploring biologically plausible learning rules for deep DendSNNs. Possible directions include difference target propagation [16] that updates parameters using locally generated activity differences, feedback alignment [17] that breaks the forward-backward symmetry constraint, and bio-inspired local plasticity based on dendritic local signals [18].

Supplementary References

- [1] Albert Gidon, Timothy Adam Zolnik, Pawel Fidzinski, Felix Bolduan, Athanasia Papoutsis, Panayiota Poirazi, Martin Holtkamp, Imre Vida, and Matthew Evan Larkum. Dendritic action potentials and computation in human layer 2/3 cortical neurons. *Science*, 367(6473):83–87, 2020.
- [2] Prajit Ramachandran, Barret Zoph, and Quoc V. Le. Searching for activation functions, 2017.
- [3] Wei Fang, Zhaofei Yu, Yanqi Chen, Tiejun Huang, Timothée Masquelier, and Yonghong Tian. Deep residual learning in spiking neural networks. In *Advances in Neural Information Processing Systems*, volume 34, pages 21056–21069, 2021.
- [4] Wei Fang, Yanqi Chen, Jianhao Ding, Zhaofei Yu, Timothée Masquelier, Ding Chen, Liwei Huang, Huihui Zhou, Guoqi Li, and Yonghong Tian. Spikingjelly: An open-source machine learning infrastructure platform for spike-based intelligence. *Science Advances*, 9(40):eadi1480, 2023.
- [5] Xundong Wu, Xiangwen Liu, Wei Li, and Qing Wu. Improved expressivity through dendritic neural networks. In *Advances in Neural Information Processing Systems*, volume 31, 2018.
- [6] Hanle Zheng, Zhong Zheng, Rui Hu, Bo Xiao, Yujie Wu, Fangwen Yu, Xue Liu, Guoqi Li, and Lei Deng. Temporal dendritic heterogeneity incorporated with spiking neural networks for learning multi-timescale dynamics. *Nature Communications*, 15(1):277, 2024.
- [7] Yu Zhang and Qiang Yang. A survey on multi-task learning. *IEEE Transactions on Knowledge and Data Engineering*, 34(12):5586–5609, 2022.
- [8] Xi Lin, Hui-Ling Zhen, Zhenhua Li, Qing-Fu Zhang, and Sam Kwong. Pareto multi-task learning. In *Advances in Neural Information Processing Systems*, volume 32, 2019.
- [9] Zhifei Zhang, Yang Song, and Hairong Qi. Age progression/regression by conditional adversarial autoencoder. In *Proceedings of the IEEE Conference on Computer Vision and Pattern Recognition (CVPR)*, pages 4352–4360, 2017.
- [10] Gregor Lenz, Kenneth Chaney, Sumit Bam Shrestha, Omar Oubari, Serge Picaud, and Guido Zarrella. Tonic: event-based datasets and transformations., 2021.
- [11] Man Yao, JiaKui Hu, Zhaokun Zhou, Li Yuan, Yonghong Tian, Bo Xu, and Guoqi Li. Spike-driven transformer. In *Advances in Neural Information Processing Systems*, volume 36, pages 64043–64058, 2023.
- [12] Jia Deng, Wei Dong, Richard Socher, Li-Jia Li, Kai Li, and Li Fei-Fei. Imagenet: A large-scale hierarchical image database. In *2009 IEEE Conference on Computer Vision and Pattern Recognition*, pages 248–255, 2009.
- [13] Tiejun Huang, Yajing Zheng, Zhaofei Yu, Rui Chen, Yuan Li, Ruiqin Xiong, Lei Ma, Junwei Zhao, Siwei Dong, Lin Zhu, Jianing Li, Shanshan Jia, Yihua Fu, Boxin Shi, Si Wu, and Yonghong Tian. 1000× faster camera and machine vision with ordinary devices. *Engineering*, 25:110–119, 2023.
- [14] Yujie Wu, Lei Deng, Guoqi Li, Jun Zhu, and Luping Shi. Spatio-temporal backpropagation for training high-performance spiking neural networks. *Frontiers in Neuroscience*, 12:331, 2018.
- [15] Timothy P Lillicrap, Adam Santoro, Luke Marris, Colin J Akerman, and Geoffrey Hinton. Backpropagation and the brain. *Nature Reviews Neuroscience*, 21(6):335–346, 2020.
- [16] Dong-Hyun Lee, Saizheng Zhang, Asja Fischer, and Yoshua Bengio. Difference target propagation. In *Machine Learning and Knowledge Discovery in Databases*, pages 498–515, 2015.
- [17] Timothy P Lillicrap, Daniel Counden, Douglas B Tweed, and Colin J Akerman. Random synaptic feedback weights support error backpropagation for deep learning. *Nature communications*, 7(1):13276, 2016.

- [18] Robert Urbanczik and Walter Senn. Learning by the dendritic prediction of somatic spiking. *Neuron*, 81(3):521–528, 2014.